



UNIwersytet Technologiczno-Przyrodniczy
Im. Jana I Jędrzeja Śniadeckich
w Bydgoszczy

ZESZYTY NAUKOWE
SCIENTIFIC JOURNAL
261

**TELEKOMUNIKACJA
I ELEKTRONIKA**
**TELECOMMUNICATIONS
AND ELECTRONICS**

16

WYDZIAŁ TELEKOMUNIKACJI
I ELEKTROTECHNIKI



BYDGOSZCZ – 2012



UNIwersytet Technologiczno-Przyrodniczy
IM. JANA I JĘDRZEJA ŚNIADECKICH
W BYDGOSZCZY

ZESZYTY NAUKOWE
SCIENTIFIC JOURNAL
261

**TELEKOMUNIKACJA
I ELEKTRONIKA**
**TELECOMMUNICATIONS
AND ELECTRONICS**

16

BYDGOSZCZ – 2012

REDAKTOR NACZELNY
prof. dr hab. inż. Józef Flizikowski

REDAKTOR NACZELNY SERII
dr inż. Beata Marciniak

OPRACOWANIE TECHNICZNE
mgr Patrycja Fereni-Morzyńska

© Copyright
Wydawnictwa Uczelniane Uniwersytetu Technologiczno-Przyrodniczego
Bydgoszcz 2012

Utwór w całości ani we fragmentach nie może być powielany
ani rozpowszechniany za pomocą urządzeń elektronicznych, mechanicznych,
kopiujących, nagrywających i innych bez pisemnej zgody
posiadacza praw autorskich.

ISSN 1899-0088

Wydawnictwa Uczelniane Uniwersytetu Technologiczno-Przyrodniczego
ul. Ks. A. Kordeckiego 20, 85-225 Bydgoszcz, tel. 52 3749482, 3749426
e-mail: wydawucz@utp.edu.pl <http://www.wu.utp.edu.pl/>

Wyd. I. Nakład 80 egz. Ark. aut. 3,7. Ark. druk. 4,6.
Zakład Małej Poligrafii UTP Bydgoszcz, ul. Ks. A. Kordeckiego 20

Contents

1. Andrzej Borys, Mariusz Aleksiewicz – COMPARISON OF DESCRIPTIONS OF CONTINUOUS-TIME AND TELETRAFFIC SYSTEMS.....	5
2. Piotr Kiedrowski, Gabriel A. Deak, Kevin Curran, Joan Condell, Bozydar Dubalski - TOWARD MORE EFFICIENT WIRELESS “LAST MILE” SMART GRID COMMUNICATION SYSTEMS.....	17
3. Marcin Szczegielniak, Damian Szczegielniak – COMPARISON OF RANGE STACKING AND OMEGA-K ALGORITHMS IN SYNTHETIC APERTURE SONAR PROCESSING.....	27
4. Łukasz Trzcianowski, Sławomir Kula – APPROACH TO QoS/QoE MONITORING AND PARAMETRIC MODEL FOR IPTV SERVICE.....	41
5. Marcin Szczegielniak, Damian Szczegielniak – OBJECTS RECOGNITION SYSTEM WITH NEURAL NETWORK	61

COMPARISON OF DESCRIPTIONS OF CONTINUOUS-TIME AND TELETRAFFIC SYSTEMS

Andrzej Borys, Mariusz Aleksiewicz

Faculty of Telecommunications and Electrical Engineering
University of Technology and Life Sciences
Kaliskiego 7, 85-789 Bydgoszcz, Poland
[andrzej.borys, mariusz.aleksiewicz]@utp.edu.pl

Summary: In a fundamental book [5] on the so-called network calculus and research papers using this technique, as for example those cited in this paper, the notion of causal linear time-invariant teletraffic systems (networks) is used. It has been mentioned in [5] that these systems are analogous to the causal linear time-invariant systems (circuits) described by integral convolution (or convolution sum in the case of discrete ones) in classical systems theory. Note that networks considered in the network calculus are described by other type of convolution that uses the infimum operation. Moreover, the algebra used in the above technique is also different. This is the so-called min-plus (or max-plus) algebra. Therefore, it is not obvious that the teletraffic systems (networks) described by the infimum convolution fulfill the following basic properties: linearity, causality, time-invariance, associativity and commutativity of their convolution operator, known from the classical theory of systems. The objective of this paper is to prove or show in detail that the above properties hold.

Keywords: Network calculus, basic properties of teletraffic systems, linearity, causality, time-invariance, associativity, commutativity, infimum convolutions

1. INTRODUCTION

Consider teletraffic system (network) which can be described by means of the so-called Network Calculus [5]. Central to the theory is the use of alternate algebras such as min-plus algebra and max-plus algebra to transform complex network systems into analytically tractable systems [4]. Many detailed examples can be found in the literature, as for example, in [1, 2, 3, 6]. The description of this system is in form of a black box, as depicted in Fig. 1, relating its output traffic $y(t)$ with its input traffic $x(t)$ through the service curve $\beta(t)$ (corresponding to the system impulse response in the classical systems theory dealing with analog or digital signals).

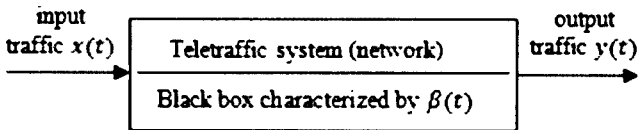


Fig. 1. A teletraffic system (network) input-output model via a black box characterized by a service curve $\beta(t)$

The input and output traffics $x(t)$ and $y(t)$, respectively, are the functions of time variable t . They have the meaning of the cumulative traffic (sums of the bits (packets) arrived in the period from 0 to t). When the relation between $y(t)$ and $x(t)$ has the form

$$y(t) = \inf_{0 \leq \tau \leq t} \{\beta(\tau) + x(t - \tau)\}, \quad \beta(\tau) \equiv 0 \text{ for } \tau < 0, \quad (1)$$

where *inf* means the mathematical operation of taking infimum value, then a system described by it is called a causal linear time-invariant one [5]. However, to our best knowledge, there is a lack of evidence in the literature, including [5], that a system described by (1) really fulfills the properties of linearity, causality and time-invariance. This paper fills the above gap. Besides, we show here how the properties mentioned look like in the case of linear systems described by an integral convolution – for reference and comparison. Finally, we compare the forms of associativity and commutativity properties of systems described by convolutions integral with those involving infimum operation.

2. LINEARITY PROPERTY

Let take into account a system described by an integral convolution of the form

$$y(t) = (Gx)(t) = G(x)(t) = \int_0^{\infty} h(\tau)x(t - \tau)d\tau, \quad h(\tau) \equiv 0 \quad (2)$$

for $\tau < 0$

where $y(t)$ and $x(t)$ represent the output and input to the system, respectively, and $h(\tau)$ is the so-called impulse response of this system. The description by (2) (as shown there) can be also expressed in the operator form $y(t) = (Gx)(t) = G(x)(t)$ with G meaning the integral convolution operator. The system represented by (2) is linear when it fulfills the following relation

$$G(ax_1 + bx_2)(t) = aG(x_1)(t) + bG(x_2)(t) = ay_1(t) + by_2(t) \quad (3)$$

where a and b are some real numbers. Moreover, $x_1(t)$ and $x_2(t)$ are two input signals, and $y_1(t)$ and $y_2(t)$ are the corresponding output ones.

Using $x(t) = a \cdot x_1(t) + b \cdot x_2(t)$ (2) gives

$$\begin{aligned}
 y(t) &= \int_0^{\infty} h(\tau)[ax_1(t-\tau) + bx_2(t-\tau)] d\tau = \\
 &= a \int_0^{\infty} h(\tau) x_1(t-\tau) d\tau + b \int_0^{\infty} h(\tau) x_2(t-\tau) d\tau = ay_1(t) + by_2(t)
 \end{aligned} \tag{4}$$

That is the linearity condition (3) is fulfilled (meaning that the systems described by integral convolutions are linear).

Consider now the systems described by (1), which is also named as infimum convolution. In this case, the algebra used is also defined differently. It is named min-plus algebra. In this algebra, the operation infimum stands for addition in the standard algebra, but the addition, on the other hand, replaces multiplication of standard algebra; for more details, see for example [5]. Therefore, here, the condition of linearity, equivalent of (3), must be written as

$$\begin{aligned}
 G\left(\inf_2 \{a + x_1(t), b + x_2(t)\}\right) &= \inf_2 \{a + G(x_1)(t), b + G(x_2)(t)\} = \\
 &= \inf_2 \{a + y_1(t), b + y_2(t)\},
 \end{aligned} \tag{5}$$

where $y_1(t) = G(x_1)(t)$ and $y_2(t) = G(x_2)(t)$ and a and b are real numbers. The subscript 2 under *inf* operation means calculation of the infimum (in this case minimum) in the set consisting of two elements. In the next step, we check whether (5) is satisfied in the case of G given by (1) or not. To this end, we substitute the signal $x(t) = \overset{inf}{2} \{a + x_1(t), b + x_2(t)\}$ into (1). This gives

$$\begin{aligned}
 y(t) &= \inf_{0 \leq \tau \leq t} \left\{ \beta(\tau) + \inf_2 \{a + x_1(t-\tau), b + x_2(t-\tau)\} \right\} = \\
 &= \inf_2 \left\{ \inf_{0 \leq \tau \leq t} \{ \beta(\tau) + a + x_1(t-\tau) \}, \inf_{0 \leq \tau \leq t} \{ \beta(\tau) + b + x_2(t-\tau) \} \right\} = \\
 &= \inf_2 \left\{ a + \inf_{0 \leq \tau \leq t} \{ \beta(\tau) + x_1(t-\tau) \}, b + \inf_{0 \leq \tau \leq t} \{ \beta(\tau) + x_2(t-\tau) \} \right\} = \\
 &= \inf_2 \{ a + y_1(t), b + y_2(t) \}
 \end{aligned} \tag{6}$$

So the linearity condition (5) is fulfilled in the case of the G operator given by (1) and min-plus algebra.

Note that in derivation of (6), we have exploited the fact that $\beta(\tau)$ is a constant in the inner expression there (second line) and interchange of *inf* operations, \inf_2 with $\inf_{0 \leq \tau \leq t}$, according to the theorem 3.1.1. ‘‘Fubini’’ formula for infimum in [5].

3. CAUSALITY

The causality property in systems theory is defined as follows: Let be two input signals x_1 and x_2 satisfying $x_1(\tau) = x_2(\tau)$ for all $\tau \leq t$. Then the operator G describing a system is called causal if it satisfies

$$y_1(t) = G(x_1)(t) = G(x_2)(t) = y_2(t) \quad (7)$$

In the case of systems described by the convolution integral (2), we have

$$\begin{aligned} y_1(t) - y_2(t) &= \int_0^{\infty} h(\tau)[x_1(t - \tau) - x_2(t - \tau)]d\tau = \\ &= - \int_t^{-\infty} h(t - \tau')[x_1(\tau') - x_2(\tau')]d\tau' = \\ &= \int_{-\infty}^t h(t - \tau')[x_1(\tau') - x_2(\tau')]d\tau' = \\ &= \int_0^t h(t - \tau')[x_1(\tau') - x_2(\tau')]d\tau' = \\ &= \int_0^t h(t - \tau') [0] d\tau' = 0 \end{aligned} \quad (8)$$

So, really, the condition (7) is fulfilled, meaning that the systems described by (2) are causal.

Note that in derivation of (8) we have used the substitution $\tau' = t - \tau$ and the fact that $h(\tau) \equiv 0$ for $\tau < 0$.

From the equality $x_1(\tau) = x_2(\tau)$ for all $\tau \leq t$, where now x_1 and x_2 mean the input traffics, and relation (1), it follows immediately that

$$\begin{aligned} y_1(t) - y_2(t) &= \\ &= \inf_{0 \leq \tau \leq t} \{\beta(\tau) + x_1(t - \tau)\} - \inf_{0 \leq \tau \leq t} \{\beta(\tau) + x_2(t - \tau)\} = 0 \end{aligned} \quad (9)$$

That is the teletraffic systems described by (1) are causal.

4. TIME-INVARIANCE

To define the time-invariance property, let us first introduce a delay operator U_T given by

$$U_T(x)(t) = x(t - T) \quad (10)$$

for signals starting at $t = 0$ that is for which $x(t) \equiv 0$ for $t < 0$. T in (10) means delaying the signal $x(t)$ by T seconds.

Generally, we say that a system described by a G operator is time-invariant if the following:

$$y_T(t) = G(x(t - T)) = G(U_T x)(t) = G(x)(t - T) = y(t - T) \quad (11)$$

holds.

Now, introducing the delayed signal $U_T(x)(t) = x(t - T)$ in (2), gives

$$\begin{aligned} y_T(t) &= \int_0^{\infty} h(\tau)x(t - T - \tau)d\tau = \\ &= \int_0^{t-T} h(\tau)x(t - T - \tau)d\tau = y(t - T) \end{aligned} \quad (12)$$

because assumptions $x(t) \equiv 0$ and $h(t) \equiv 0$ for $t < 0$ follow that only the times $t - T - \tau > 0$ and $\tau > 0$ make sense. This leads to the upper limit in the integral $t - T$ and $t > T$. Otherwise, $y_T(t) \equiv 0$. Finally, we conclude that relation (12) proves the time-invariance of systems described by the integral convolution (2).

Consider now the teletraffic systems described by (1) and introduce there the delayed input traffic $x(t - T)$ (given by similar expression as (10)). We get then

$$y_T(t) = \inf_{0 \leq \tau \leq t} \{\beta(\tau) + x(t - T - \tau)\} \quad (13)$$

Furthermore, note that the restrictions regarding (13) are similar to those occurring in the previous case, that is $t - T - \tau > 0$ and $\tau > 0$. They lead to the upper limit $t - T$ instead of t under the symbol \inf in (13) and the inequality $t > T$. Otherwise, $y_T(t) \equiv 0$. So, from (13) we get

$$y_T(t) = \inf_{0 \leq \tau \leq t-T} \{\beta(\tau) + x(t - T - \tau)\} = y(t - T) \quad (14)$$

which proves the time-invariance property of teletraffic systems described by (1).

5. ASSOCIATIVITY AND COMMUTATIVITY OF INTEGRAL AND INFIMUM CONVOLUTION

Associativity and commutativity of the integral convolution are very useful properties exploited in calculations. Let us recall their derivation here, especially, that the derivation of the first one is not obvious.

We begin with the commutativity property, which proves immediately, when we apply the assumption $x(t) \equiv 0$ for $t < 0$, introduce a new variable

$\tau' = t - \tau$, rename τ' as τ , and finally take into account the fact that $h(t) \equiv 0$ for $t < 0$. In effect, we get from (2)

$$\begin{aligned}
 y_T(t) &= \int_0^{\infty} h(\tau)x(t-\tau)d\tau = \int_0^t h(\tau)x(t-\tau)d\tau = \\
 &= -\int_t^0 h(t-\tau')x(\tau')d\tau' = \int_0^t x(\tau')h(t-\tau')d\tau' = \\
 &= \int_0^t x(\tau)h(t-\tau)d\tau = \int_0^{\infty} x(\tau)h(t-\tau)d\tau
 \end{aligned} \tag{15}$$

Consider now a cascade of two systems characterized by their impulse responses $h_1(t)$ and $h_2(t)$ as depicted in Fig. 2, with $x(t)$ being the input signal to the cascade and the corresponding output signals $y_1(t)$ and $y_2(t)$.

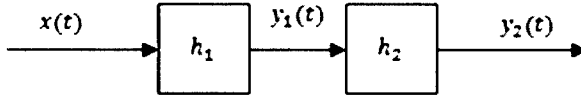


Fig. 2. A cascade of two systems for illustration of associativity property

To proceed further, observe first that according to (15) the descriptions

$$\int_0^{\infty} h(\tau)x(t-\tau)d\tau \quad \text{and} \quad \int_0^t h(\tau)x(t-\tau)d\tau$$

in our setting, are equivalent to each other. In what follows, we shall use the latter. So, for the cascade in Fig. 2, using additionally the commutativity property (15), we can write

$$\begin{aligned}
 y_2(t) &= \int_0^t y_1(\tau_2) h_2(t-\tau_2)d\tau_2 = \\
 &= \int_0^t \int_0^{\tau_2} x(\tau_1)h_1(\tau_2-\tau_1)h_2(t-\tau_2)d\tau_1d\tau_2
 \end{aligned} \tag{16a}$$

Associating h_1 with h_2 would give

$$h(t-\tau_1) = \int_0^{t-\tau_1} h_2(\tau_3) h_1(t-\tau_1-\tau_3)d\tau_3 \tag{16b}$$

and then it should be possible to express $y_2(t)$ as

$$y_2(t) = \int_0^t x(\tau_1) h(t - \tau_1) d\tau_1 \tag{16c}$$

With $h(\cdot)$ given by (16b). In what follows, we will answer whether the above is true. For this purpose, consider an area of iteration of the double iterated integral occurring in (16a). It is illustrated in Fig. 3, and follows from the fact in our setting $h_1(t) \equiv 0$, $h_2(t) \equiv 0$ and $x(t) \equiv 0$ for all $t < 0$. This gives $t \geq \tau_2 \geq \tau_1 \geq 0$.

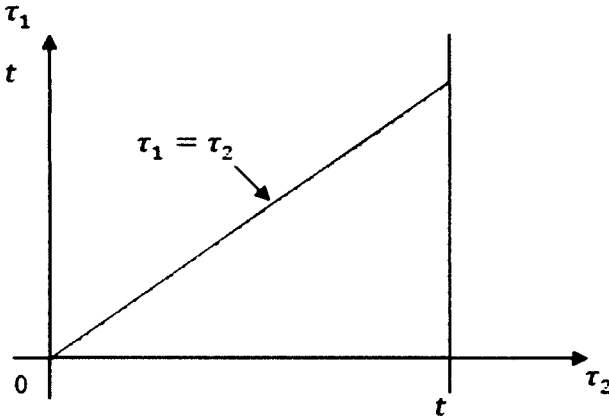


Fig. 3. The area of integration of an iterated integral in (16a)

Introduction of a new variable $\tau_3 = t - \tau_2$ rearranges the set of inequalities $t \geq \tau_2 \geq \tau_1 \geq 0$ to $t \geq \tau_1 \geq 0$ and $t - \tau_1 \geq \tau_3 \geq 0$, which describes a new area of integration (with τ_3 instead of τ_2). This area is shown in Fig. 4.

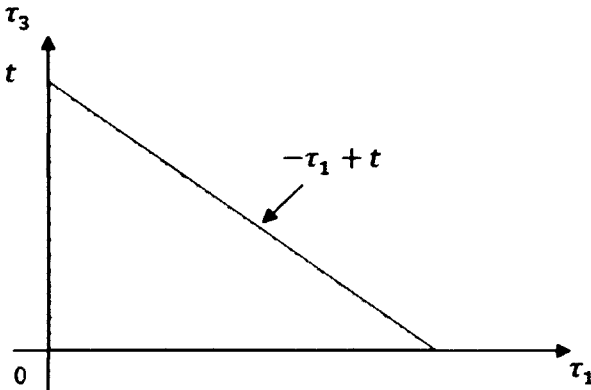


Fig. 4. The area of integration of an iterated integral in (16a) after introducing a new variable τ_3 instead of τ_2

Taking into account in (16a) the area of integration shown in Fig. 4, we arrive at

$$\begin{aligned}
 y_2(t) &= \int_0^t \int_0^{t-\tau_1} x(\tau_1) h_1(t - \tau_1 - \tau_3) h_2(\tau_3) d\tau_3 d\tau_1 = \\
 &= \int_0^t x(\tau_1) \int_0^{t-\tau_1} h_1(t - \tau_1 - \tau_3) h_2(\tau_3) d\tau_3 d\tau_1
 \end{aligned} \tag{17}$$

Further, we deduce from (17) that, really, the output signal $y_2(t)$ can be expressed as in (16c) with $h(t)$ given by (16b). And this finally proves the associativity property of the integrated convolution given by (2).

Consider now the question of commutativity of the infimum convolution defined in (1). Introducing in (1) a new variable $\tau' = t - \tau$ gives

$$\begin{aligned}
 y(t) &= \inf_{0 \leq \tau \leq t} \{\beta(\tau) + x(t - \tau)\} = \inf_{0 \leq \tau' \leq t} \{\beta(t - \tau') + x(\tau')\} = \\
 &= \inf_{0 \leq \tau \leq t} \{x(\tau) + \beta(t - \tau)\}
 \end{aligned} \tag{18}$$

with τ' renamed as τ in the last equality in (18). Looking at (18), we see that, really, the infimum convolution is commutative.

To show that the associativity property holds in the case of infimum convolution we need to prove first the following theorem.

Theorem 1. Let $S = S(\tau_1, \tau_2)$ be a set consisting of pairs of $\tau_1, \tau_2 \in R$ and let $S_{\tau_2}(\tau_1)$ and $S_{\tau_1}(\tau_2)$ be subsets of $S(\tau_1, \tau_2)$ chosen such that τ_2 or τ_1 , respectively, is constant. Then, the following

$$\inf_{\tau_2 \in S} \left\{ \inf_{\tau_1 \in S} \left\{ f \left(S_{\tau_2}(\tau_1) \right) \right\} \right\} = \inf_{\tau_1 \in S} \left\{ \inf_{\tau_2 \in S} \left\{ f \left(S_{\tau_1}(\tau_2) \right) \right\} \right\} \tag{19}$$

holds, where $f(\cdot)$ is a function of τ_1 and τ_2 belonging to the set S .

Proof. Using the notation introduced above, we can write the range of the function f as range of

$$f = f(S) \tag{20}$$

Furthermore, note that

$$S = S(\tau_1, \tau_2) = \bigcup_{\tau_2 \in S} S_{\tau_2}(\tau_1) = \bigcup_{\tau_1 \in S} S_{\tau_1}(\tau_2) \tag{21}$$

Applying now the infimum operation to the set given by (20) with (21), we obtain

$$\begin{aligned} \inf\{f(S)\} &= \inf_{\tau_1, \tau_2 \in S} \{f(S(\tau_1, \tau_2))\} = \inf_{\tau_1, \tau_2 \in S} \left\{ \bigcup_{\tau_2 \in S} S_{\tau_2}(\tau_1) \right\} = \\ &= \inf_{\tau_2 \in S} \left\{ \inf_{\tau_1 \in S} \{f(S_{\tau_2}(\tau_1))\} \right\} \end{aligned} \quad (22a)$$

or, similarly,

$$\inf\{f(S)\} = \inf_{\tau_1 \in S} \left\{ \inf_{\tau_2 \in S} \{f(S_{\tau_1}(\tau_2))\} \right\} \quad (22b)$$

Therefore, we can conclude that the expressions on the most right-hand sides of (22a) and (22b) are equal each to other, and this constitutes the equality (19).

Concluding, we say that one can interchange the subscripts τ_1 and τ_2 in the way as shown in (19), when performing infimum operation iteratively. Moreover, note that our theorem 1 is generalization of the theorem 3.1.1 ‘‘Fubini’’ formula for infimum presented in [5] for any set consisting of two variables τ_1 and $\tau_2 \in R$.

Consider now a cascade of two teletraffic systems as shown in Fig. 5.

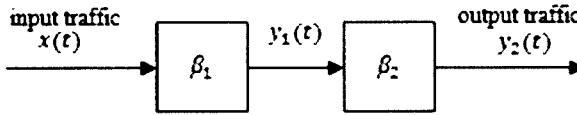


Fig. 5. A cascade of two teletraffic systems for illustration of associativity property

$$\begin{aligned} y_2(t) &= \inf_{0 \leq \tau_2 \leq t} \{\beta_2(\tau_2) + y_1(t - \tau_2)\} = \\ &= \inf_{0 \leq \tau_2 \leq t} \left\{ \beta_2(\tau_2) + \inf_{0 \leq \tau_1 \leq t - \tau_2} \{\beta_1(\tau_1) + x(t - \tau_2 - \tau_1)\} \right\} = \\ &= \inf_{0 \leq \tau_2 \leq t} \left\{ \inf_{0 \leq \tau_1 \leq t - \tau_2} \{\beta_2(\tau_2) + \beta_1(\tau_1) + x(t - \tau_2 - \tau_1)\} \right\} = \\ &= \inf_{0 \leq \tau_2 \leq t} \left\{ \inf_{0 \leq \tau_1 \leq t - \tau_2} \{\beta_2(\tau_2) + \beta_1(t - \tau_2 - \tau_1) + x(\tau_1)\} \right\} \end{aligned} \quad (23)$$

Note that the last expression in (23) holds because $\beta_2(\tau_2)$ does not depend upon τ_1 . Moreover, the commutativity property of the infimum convolution has been used in it.

In the next step, we introduce a new variable $\tau'_1 = t - \tau_1$ in (23). This leads to

$$\begin{aligned}
 y_2(t) &= \inf_{0 \leq \tau_2 \leq t} \left\{ \inf_{\tau_2 \leq \tau_1 \leq t} \{ \beta_2(\tau_2) + \beta_1(\tau_1 - \tau_2) + x(t - \tau_1) \} \right\} = \\
 &= \inf_{0 \leq \tau_1 \leq t} \left\{ x(t - \tau_1) + \inf_{0 \leq \tau_2 \leq \tau_1} \{ \beta_2(\tau_2) + \beta_1(\tau_1 - \tau_2) \} \right\}
 \end{aligned} \tag{24}$$

Note that the interchange of the subscript τ_2 and τ_1 under the infimum operations in (24) have been used, according to theorem 1. And finally, we conclude that (24) proves fulfillment of the associativity property by the infimum convolution.

6. DIGITAL SIGNAL-BASED SYSTEMS

The digital linear time-invariant causal systems are described by a sum convolution as

$$y(k) = \sum_{i=0}^{\infty} h(i)x(k-i), \quad \text{with } h(i) \equiv 0, \quad x(i) \equiv 0 \text{ for } i < 0 \tag{25}$$

in place of the integral convolution for time-continuous systems. In (25), $h(\cdot)$, $y(\cdot)$ and $x(\cdot)$ are the samples of the system impulse response, its output signal, and its input signal, respectively. Moreover, k means a discrete time.

Also the systems characterized by (25) possess the properties we dealt with in the previous section. This can be easily shown using the approach applied before for analogous ones.

7. CONCLUSION

In this paper, we have analyzed systematically the basic properties of teletraffic systems that can be described by an infimum convolution. We have shown that these systems are linear, causal, and time-invariant. Moreover, their convolution operator fulfills the properties of associativity and commutativity. To our best knowledge, the derivations presented here have not been presented in the literature, at least in such a systematic form. For reference and comparison, we have also presented analogous derivations for systems of which input-output descriptions are in form of an integral convolution.

BIBLIOGRAPHY

- [1] Agrawal R., Cruz R. L., Okino C., Rajan R., 1999, Performance Bounds for Flow Control Protocols. IEEE/ACM TRANSACTIONS ON NETWORKING, Vol. 7, No. 3.

- [2] Fidler M., 2010, A Survey of Deterministic and Stochastic Service Curve Models in the Network Calculus. IEEE COMMUNICATIONS SURVEYS & TUTORIALS, Vol. 12, No. 1.
- [3] Ghiassi Y., Liebeherr J., 2009, Output Characterization of Constant Bit Rate Traffic in FIFO Networks. IEEE COMMUNICATIONS LETTERS, Vol. 13, No. 8.
- [4] Jiang Y., 2009, Network Calculus and Queueing Theory: Two Sides of One Coin. VALUETOOLS, Pisa, Italy.
- [5] Le Boudec J.-Y., Thiran P., 2004, Network Calculus. A Theory of Deterministic Queueing Systems for the Internet. Springer Verlag, Berlin, Germany.
- [6] Liebeherr J., Valaee S., 2010, A system-Theoretic Approach to Bandwidth Estimation. IEEE/ACM TRANSACTIONS ON NETWORKING, Vol. 18, No. 4.

PORÓWNANIE OPISÓW SYSTEMÓW TELEINFORMATYCZNYCH ORAZ CIĄGLYCH W CZASIE

Streszczenie

W znanej monografii nt. rachunku sieciowego (network calculus), napisanej przez J.-Y. Le Boudeca i P. Thirana, zostało wprowadzone pojęcie liniowych systemów teleinformatycznych niezależnych od czasu. Wskazano w niej na podobieństwa istniejące pomiędzy powyższą klasą systemów a liniowymi systemami analogowymi niezależnymi od czasu, jednakże zrobiono to w sposób dosyć pobieżny. W tym artykule podobieństwa te są przeanalizowane w sposób systematyczny, a także bez uciekania się do bardzo abstrakcyjnej teorii systemów opisywanych za pomocą algebry min-plus – jedynie przy wykorzystaniu elementarnych pojęć matematyki wyższej. Wiele przedstawionych tutaj wyprowadzeń nie było dotychczas nigdzie publikowanych, jak na przykład twierdzenie 1.

Słowa kluczowe: rachunek sieciowy (network calculus), liniowe i niezależne od czasu systemy teleinformatyczne, własności splotu w algebrze min-plus

TOWARD MORE EFFICIENT WIRELESS “LAST MILE” SMART GRID COMMUNICATION SYSTEMS

Piotr Kiedrowski¹, Gabriel A. Deak², Kevin Curran²,
Joan Condell², Bozydar Dubalski¹

¹Institute of Telecommunication, University of Technology and Life Science
Kaliskiego 7, 85-789 Bydgoszcz, Poland

²ISRC – University of Ulster. Magee Campus. Northland Rd., BT48 7JL. Derry, UK

Summary: Multi-hop techniques are very popular in Wireless Sensor Networks as they are used to solve coverage problems. The drawback of these techniques is the low reliability. The aim of this paper is to outline hardware solutions that improve the efficiency of wireless networks intended for “last mile” smart grid communication systems. Typical Wireless Sensor Networks cannot take advantage of these solutions due to power constraints. Fast carrier detection and the probability of collisions, forward error correction, data whitening, and clear channel assessment are discussed as hardware solution to improve wireless network efficiency for “last mile” smart grid communication systems. The hardware solutions significantly improve the efficiency of the wireless network intended for “last mile” smart grid communication systems.

Keywords: smart grid, wireless sensor network, last mile communication, PER vs. RSSI

1. INTRODUCTION

Successful implementation of Smart Grid (SG) solutions depend mostly on the adopted communication solutions [1]. Currently, the main problem in the implementation of Smart Grid communication systems is the solution of the “last mile”, part of SG communication networks. This part of networks has a decisive impact on the cost of implementation and operation of the whole communication system. Thus very cheap sensor-based devices have been used to deploy “last mile” wireless networks. Wireless Sensor Networks (WSNs) use similar hardware solutions.

A typical node in a WSN consists of an antenna, a microcontroller, a transceiver and a sensor. In Europe, microwaves with frequencies 433 MHz and 868 MHz (ISM - Industrial, Scientific, Medical radio band) are very often used for automatic meter reading (AMR) systems and WSNs. Nodes using these frequencies have a maximum transmission power of approximately 10 dBm and

a short transmission range. In order to increase the transmission range a multi-hop technique is often used. Thus a node in a network may act as a source node, destination node, or a transfer node. The only difference between typical WSN nodes and SG nodes is the power supply. WSN nodes are powered by small batteries whilst SG ones are powered directly from mains electricity monitored by this node. If there are no power constraints we can implement different system solutions e.g. communications protocols or topology control. System solutions are mainly realized by software methods. However, the best results in improving the efficiency of the network are obtained by using the software and hardware solutions simultaneously.

In this paper we have proposed four hardware solutions such as fast carrier detection, forward error correction, data whitening and clear channel assessment. The hardware solutions significantly improve the efficiency of the wireless network intended for “last mile” smart grid communication systems. These solutions cannot be applied in typical WSN where the nodes have power constraints.

2. FAST CARRIER DETECTING AND COLLISIONS PROBLEM

Using a multi-hop technique, the reliability of the path between source and destination nodes is based on individual reliability of all nodes in the path. The Packet Error Ratio (PER) value is high for communications between sensor-based devices compared to other types of communication media e.g. optical fiber.

Multi-hop techniques are very popular in WSN. These techniques solve the coverage problem. However wireless communications using these techniques have low reliability. A solution to cope with the high PER value is fairly easy to implement when we do not have to consider energy efficiency. A multipath routing protocol [2], using more than one path between source and destination nodes at the same time, could fix the problem. Multipath routing protocol is wasting more energy but this is not a problem in proposed application. However, generating many redundant transmissions still seems to be a problem. This can be evaluated as the probability of sending two or more packets at the same time, using the equation below:

$$P_c(k, T, t) = 1 - \frac{\left(\frac{T}{t}\right) \cdot \left(\frac{T}{t} - 1\right) \cdot \dots \cdot \left(\frac{T}{t} - k + 1\right)}{\left(\frac{T}{t}\right)^k} \quad (1)$$

where:

- k is the number of nodes in a cluster, transferring a packet in a defined hop.
- t shows how long the CD (Carrier Detect) status cannot be monitored,
- T is a maximum value of random time delay in the process of packet reliability.

The value of P_c could be decreased by increasing the value of T if there was no influence on the communication time. Similarly, P_c could be decreased by decreasing the value of k , but we have no influence on the network topology. The only possibility to decrease the value of P_c is to reduce the time t . Fig. 1 presents the probability of collisions for three values of t based on the number of nodes k .

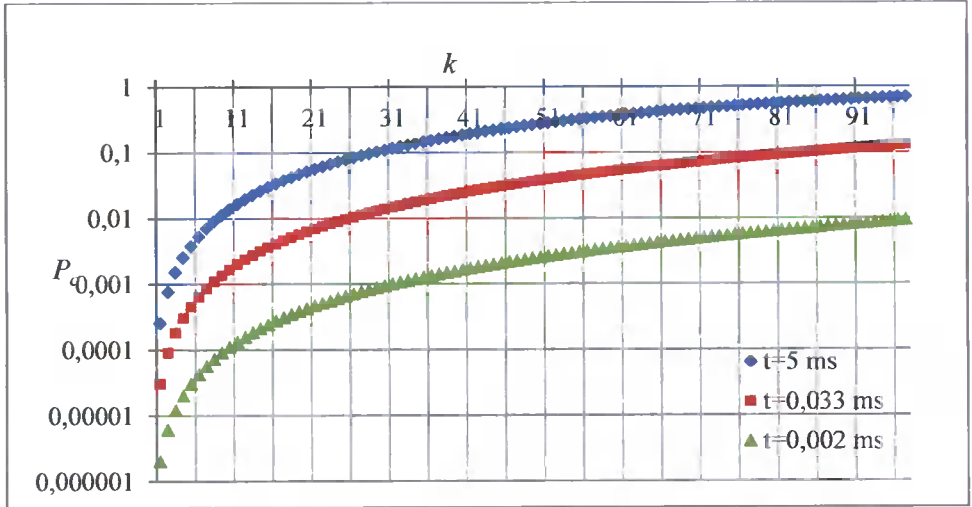


Fig. 1. Probability of collisions vs. the number of nodes in transferring cluster

Equation 1 was used to obtain the results in Figure 1 for a constant value of T equal to 1 s. The value of t is the time needed to detect status of carrier (if channel is busy or free). Usually radio modules have clocks factory set only to 32 kHz. This is because radio modules are mainly intended to work in WSNs, where the power conservation is the main issue. In this case, when clock is slow, the time needed to detect CS is long e.g. 5 ms if it is readout via SPI (Serial Peripheral Interface). When the same module is overclocked up to 5 MHz the information about CS is achievable in about 33 μ s. The last example, which is also presented in Fig. 1, concerns the same module with both the overclocked microcontroller and additionally with the CD output pin of the transceiver connected directly to the IRQ input pin of the microcontroller. With such modifications $t=2 \mu$ s. Assuming that the probability of a collision cannot be greater than 0.01, the maximum number of nodes transferring the same packets should not exceed 9 if hardware solutions allow microcontrollers to detect a carrier with sense of 5 ms. The main reason of using the 0.01 threshold value is the fact that many applications use this value as the unreliability measure in order to calculate threshold parameters. In [3] the value $PER=10^{-2}$ was obtained using this threshold value as the probability of collision. This time is too short considering that 9 nodes or bigger clusters occur very often. By using a module with an

overclocked microcontroller, we can detect carrier faster. In this case we have the possibility to obtain a probability of collision less than 0.01 if the size of transferring cluster is smaller than 27 nodes. The case when the number of nodes in a cluster is greater than 27 is rare. The whole subnet (managed by one sink) contains at most a few hundred nodes spread over a large area. Thus, it can be concluded that in this case, when the network is merely energy meters, using an overclocked radio module is sufficient when multi-hop and multipath transmission technique are used. In the future if SG systems usage will increase then the number of nodes in the network will increase several times. In this case, the third solution will be necessary to ensure a low probability of collisions in clusters consisting of more than one hundred nodes.

3. HARDWARE FORWARD ERROR CORRECTION

Most of the one-chip transceivers on the market have built in support for forward error correction (FEC). By using this option the energy consumption increases. This is the main reason why FEC is not a very popular technique for improving the transmission parameters in typical WSN solutions. FEC is a good choice when energy efficiency is not a concern.

In order to see if this option improves the efficiency of transmission we ran an experiment where we alternate sending and receiving packets on the network – odd packets with FEC, even without FEC.

The efficiency of transmission can be assessed by various methods. The most popular methods are the quality of service assessment and the reliability of links measurement. The quality of service method is a direct method and is dedicated to specific solutions e.g. implemented communication scheme. The second method is more general and estimates the quality of service when the implemented solutions are known. The efficiency of transmission with FEC was assessed using these two methods.

As a measure of the quality of service we have considered the data collection speed (number of readings from nodes per time interval) for all the nodes in our test network. The speed increased with 9% using FEC compared to the case when FEC was off.

We have also measured the PER versus Received Signal Strength Indicator (RSSI) in the neighbourhood of the sink, based on all data received by the sink. We cannot plot both $PER_{FEC}(RSSI)$ and $PER_{noFEC}(RSSI)$ in the same graphics as curves overlap. During long-term tests the results were always better using FEC compared to the case without FEC. The global values of PER (regardless of RSSI) were as follow: $PER_{FEC} = 9.92 \cdot 10^{-2}$ and $PER_{noFEC} = 1.08 \cdot 10^{-1}$.

We expected that the use of FEC would improve the transmission. However the difference compared to the case without FEC was not large enough to help us assess the transmission based on PER. Such a situation is the effect of

the implemented communication scheme on the function of the relative PER growth versus RSSI, expressed by the following equation:

$$\delta PER_{noFEC,FEC}(RSSI) = \frac{PER_{noFEC}(RSSI) - PER_{FEC}(RSSI)}{PER_{FEC}(RSSI)} = \frac{PER_{noFEC}(RSSI)}{PER_{FEC}(RSSI)} - 1 \quad (2)$$

Figure 2, obtained using (2), shows the influence of FEC on the transmission reliability.

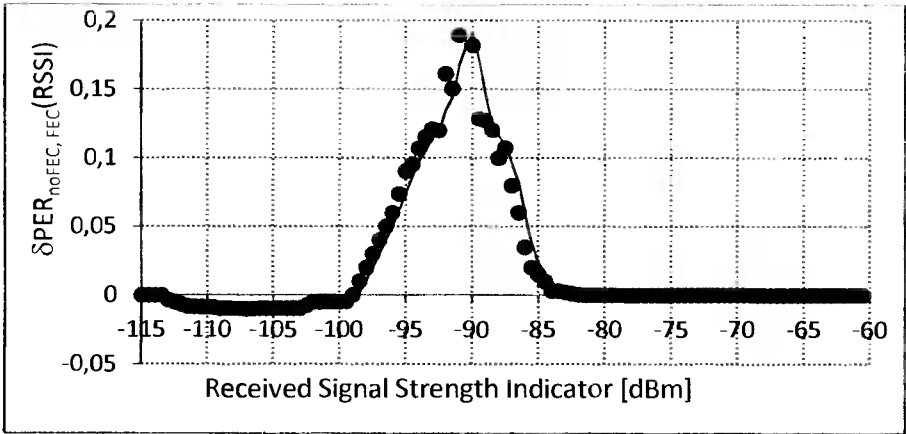


Fig. 2. The influence of FEC on the transmission reliability – relative PER versus RSSI

Four power ranges can be distinguished analysing the data in Fig. 2. The first power range is for RSSI values less than -113 dBm. In this range all packets have errors with or without using FEC.

The second power range is for RSSI values between -113 dBm and -99 dBm. In this range the value of the relative PER is less than zero. This means the FEC function does not improve transmission but worsens it instead. This situation can be easily explained taking into account the range of RSSI. The signal received by a sink is very weak which means the nodes are located on the edge of their radio range. When the FEC is switched off, nodes located on the edge do not receive packets from the sink or receive packets with errors, thus do not send copies. However, when the FEC is switched on, some nodes receive error free packets from the sink and send copies to other nodes. This improves the communication but does not improve the relative PER measured at the sink point.

The third power range is for RSSI values between -99 dBm and -82 dBm. In this range the value of the relative PER is greater than zero and it goes up to nearly 20% for -90 dBm, thus the FEC function improves transmission.

The fourth power range is for RSSI values greater than -82 dBm. In this range all packets are error free and do not depend on the status of the FEC function.

Concluding, we can say that only in the power range between -99 dBm and -82 dBm is the FEC function significantly effective. We can also say that in the power range between -113 dBm and -99 dBm, FEC is only seemingly in effective. In other power ranges FEC function does not affect the PER. Nevertheless, the FEC function can be very useful under conditions of interferences especially in the fourth power range. This phenomenon was explained based on the observations presented in [4].

4. DATA WHITENING

In the ideal case, over many different types of media, random DC-free (Direct Current) data is transmitted. In many cases the data transmitted contains long sequences of ones and/or zeros. Performance can then be improved by whitening the data (DW) before transmitting and de-whitening at reception.

The data is prepared by applying exclusive-or (XOR) with a pseudo-random sequence before transmission. Results in this paper were obtained using pseudo-random bit sequences generated by the polynomial function $G(x)=x^9+x^5+1$. This method is called data whitening. When the data is received, it is XOR'd with the same pseudo-random sequence to obtain the original data. Fig. 3 presents a circuit for data whitening:

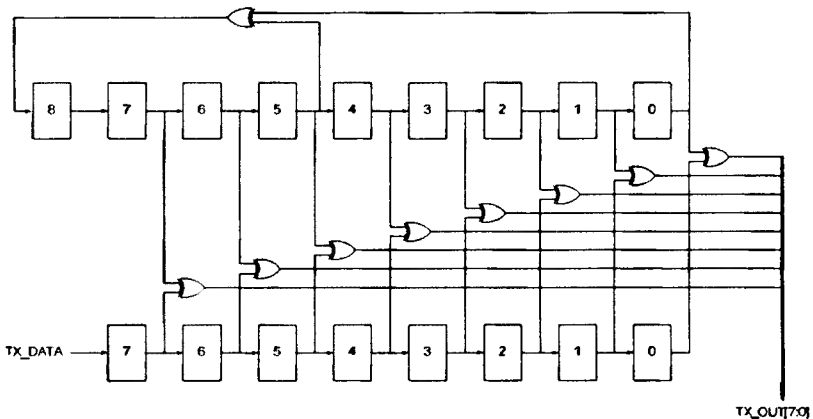


Fig. 3. Data whitening circuitry [5]

Figure 3 shows a circuit for data whitening similar to the scrambler circuit implemented in SONET/SDH optical communication technology to realize the same function as a line coding i.e. avoiding of long sequences of zeros or ones.

Using a similar technique as in the examination of the FEC, i.e. alternate sending and receiving packets we have analysed the improvement on the transmission efficiency by alternating the usage of DW with the case when DW is not used. However the DW function had no effect on the transmission efficiency, either on readings speed or PER

One should not consider our results as general due to the specific telemetric data organized in packets. The packets, which carried telemetric data, consist of the overhead and the data field. The data fields are encrypted so they are already random and do not need to be whitened. The overhead consist mostly of long addresses which rarely contain long sequences of zeros and never contain long sequences of ones, where an address is a real serial number of a device coded in BCD.

5. CLEAR CHANNEL ASSESSMENT

The Clear Channel Assessment (CCA) is used to indicate if the channel is free or busy, during the transmitting process. There are different criteria for determining whether the channel is free or busy such as: RSSI is below threshold, receiver currently is receiving a packet etc.

The CCA function is very useful if the point-to-point transmission mode is used with a half-duplex transmission channel. The CCA function can be also useful when we use not advanced routing protocols e.g. flooding [6] or gossip [7], whilst when we use advanced routing protocols e.g. energy greedy quasi-flooding (EGQF) routing protocol [8], which is used in our test network, the usage of the CCA is not recommended.

This is because, even though, during the transmitting process with CCA enabled, the receiver is in RX state, it cannot receive any packet but just wait for an opportunity to transmit the own, hold in TX buffer, packet as soon as channel is free. Using advanced transmission techniques, the information which is waiting to be sent can be out-of-dated by received one. So, we recommend using the CCA feature only for a simple e.g. ping-pong transmission systems in order to shorten the time of an idle state required between receiving and transmitting states.

Examining the CCA in our test network, the CCA function had no effect on the transmission efficiency but had a negative effect of increasing the average rate of transmitted packets per query.

CONCLUSIONS

Most of the single chip transceivers have many internal modules which can be programmatically switched on or off. However the drawback of using additional modules is increased power consumption, therefore developers often have to opt out of using additional/optional possibilities offered by modern communication chips.

In the case of systems with no energy deficit (e.g. SG) one can use other solutions, both hardware and software. Here, however, the risk is that the designers decide to include all internal modules aimed at improving the transmission parameters. The article shows that by deciding to include any additional function, one has to take into account not only energy consumption but also the protocols used by the systems such as communication protocols.

Transmission parameters and quality of service were compared for two cases, the first with optional functions enabled and the second with optional functions disabled. Comparison of transmission parameters and quality of service with all features enabled or disabled is not presented. Such an experiment was not performed, because a solution that has the greatest impact on transmission parameters and network performance is a fast carrier sensing. Other functions have a significant effect only when the CS detection is not fast enough. Therefore a fast carrier detecting solution is the most important and must be taken into account at the stage of hardware design. Usage of other solutions depends strongly on the system to be implemented and the characteristics of this system should be considered before switching on optional features.

BIBLIOGRAPHY

- [1] IEEE SmartGridComm 2011 Concludes, Successful 2nd Annual Event in Brussels, Belgium, IEEE Communications Magazine, Conference Report, December 2011, pp. 18-19.
- [2] Al-Karaki A.N., Kamal A.E., Routing Techniques in Wireless Sensor Networks: a Survey, IEEE Wireless Comm., Dec. 2004 (2004), 6-28.
- [3] Texas Instruments (2006) CC1100 Single Chip Low cost Low Power RF Transceiver. Texas Instruments Incorporated, 89-90.
- [4] Boryna B., Dubalski B., Kiedrowski P. and Zabłudowski A.: Image Processing and Communications Challenges 2 (ed. Ryszard S. Choraś), Errors Nature in Indoors Low Power 433 MHz Wireless Network, 2010 Springer Verlag, Advances in Intelligent and Soft Computing 84, pp. 373-378.
- [5] Grant Christiansen: Data Whitening and Random TX Mode, Texas Instruments, 2010.
- [6] Durrresi A., Paruchuri V.K., Iyengar S.S., Kannan R.: Optimized Broadcast Protocol for Sensor Networks, IEEE Transactions on Computers, Vol. 54, No. 8, August 2005, pp. 1013-1024.
- [7] Boyd S., Ghosh A., Prabhakar B., Shah D.: Randomized Gossip Algorithms, IEEE Transactions on Information Theory, Vol. 52. No. 6. June 2006, pp. 2508-2530.
- [8] Kiedrowski P., Dubalski B., Marciniak T., Riaz T. and Gutierrez J.: Image Processing and Communications Challenges 3 (ed. Ryszard S. Choraś), Energy Greedy Protocol Suite for Smart Grid Communication Systems Based on Short Range Devices, 2011 Springer Verlag, Advances in Intelligent and Soft Computing 102, pp. 493-502.

KU BARDZIEJ WYDAJNYM SIECIOM BEZPRZEWODOWYM "OSTATNIEJ MILI" PRZEZ INTELIGENTNE SYSTEMY KOMUNIKACJI W SIECI

Streszczenie

Technika transmisji multi-hop jest powszechnie stosowana w bezprzewodowych sieciach sensorowych w celu powiększenia zasięgu jej działania. Jednak wadą techniki multi-hop jest duża zawodność transmisji. Celem artykułu jest przedstawienie sprzętowych metod poprawy jakości transmisji w bezprzewodowych sieciach sensorycznych przeznaczonych do obsługi komunikacji w systemach Smart Grid w obszarze ostatniej mili. Prezentowane w pracy metody nie są stosowane w klasycznych bezprzewodowych sieciach sensorowych ze względu na deficyt energii charakterystyczny dla sieci, których węzły zasilane są bateryjnie. Prezentowane metody oraz ich skuteczność dotyczą takich zagadnień, realizowanych metodami sprzętowymi, jak: szybkie wykrywanie sygnału nośnej, korekcja błędów wprzód, uprzypadkawianie strumienia danych, kryterium decyzji o transmisji CCA (ang. clear channel assessment). W pracy w sposób teoretyczny i praktyczny wykazano skuteczność proponowanych metod.

Słowa kluczowe: sieci Smart Grid, sieci sensorowe, komunikacja ostatniej mili, PER vs RSSI

COMPARISON OF RANGE STACKING AND OMEGA-K ALGORITHMS IN SYNTHETIC APERTURE SONAR PROCESSING

Marcin Szczegielniak¹, Damian Szczegielniak²

University of Technology and Life Sciences,
Kaliskiego 7, Bydgoszcz 85-796 Poland

¹szczegielniakm@wp.pl, ²dszczeg@utp.edu.pl

Summary: Synthetic Aperture Sonar (SAS) processing is continuously developing into a direction of better, more effective and accurate algorithms. It is preferable to use algorithms which don't introduce additional errors because of a phase approximation or digital data interpolation. One of them is Range Stacking. The short analysis of this algorithm, emphasizing its advantages and disadvantages in comparison with another reconstruction algorithm called Omega-k, was carried out in the paper. The simulated raw SAS signals for the stripmap mode were the basis of the practical part of the comparison. The set of examined SAS images included some signals after the spatial filtering with the use of Polar Format Processing. The results of the numerical simulation are shown and discussed in this paper.

Keywords: synthetic aperture sonar, range stacking, omega-k, comparison

1. INTRODUCTION

A stripmap SAS system in the three-dimensional spatial (x,y,z) domain during the data acquisition is depicted in Fig. 1A. The SAS system sends successive sound pulses perpendicular to the direction of the travel (the broadside case). The positions of the platform (where pulses are transmitted and received) are evenly spaced. This is because a constant Pulse Repetition Frequency (PRF) as well as a constant platform speed are assumed. The platform position and system parameters determine the size and shape of the aperture footprint on seafloor's surface. This footprint is swept along-track as the platform moves along ping by ping, illuminating the swath, so that the response of a scatterer on the seafloor is included in more than single sonar echo. An appropriate coherent combining of the signal returns (by means of a SAS reconstruction algorithm) leads to the formation of synthetically enlarged antenna of the length $2L$ (Fig. 1B), what is equivalent to obtaining a high-resolution reflectivity map of an acoustic backscatter strength.

The assumed ‘stop and hop’ model (the sonar is stationary between transmitting and receiving signals) is not particularly valid in real conditions because of the relatively low sound speed in water (in comparison with the propagation of electromagnetic waves and thus SAR systems). However, it seems to be good enough to compare two different SAS reconstruction algorithms and gets more appropriate for SAS systems operating at short target ranges (Tab. 1). No motion errors influence is taken into account in this paper. In order to simplify later analysis it’s possible to define the new variable

$$r = \sqrt{y^2 + h^2} \quad (1)$$

where h is the altitude of the platform and y denotes the spatial coordinate according to Figure 1A. Thanks to this abbreviation the imaging scene can be represented by the two-dimensional spatial (x, r) domain. The synthetic aperture domain will be represented by the variable x' in order to distinguish from the coordinate x . A signal transmitted by an antenna can be written as

$$p_{tr}(t) = p(t) \cdot \exp[i\omega_c t] \quad (2)$$

where $p(t)$ and ω_c denote Linear Frequency Modulated (LFM) signal and a carrier frequency respectively. After receiving and demodulation the echo signal from the scatterer located at (x, r) , assuming the lossless environment, we have

$$e(x', t) = \sigma \cdot p \left(t - \frac{2\sqrt{(x - x')^2 + r^2}}{c} \right) \exp \left[-i\omega_c \cdot \frac{2\sqrt{(x - x')^2 + r^2}}{c} \right] \quad (3)$$

where c is the sound speed in water, σ represents unknown reflectivity coefficient and x' is the position of the platform (synthetic aperture).

The examined Range Stacking and Omega-k belong to the same group of relatively modern reconstruction algorithms which are free of Fresnel approximation errors [2]. However, the Range Stacking algorithm does not require any interpolation and thus it does not suffer from the truncation errors. Either one is used in high-resolution imaging SAR or SAS systems as the reconstruction step in synthetic aperture processing.

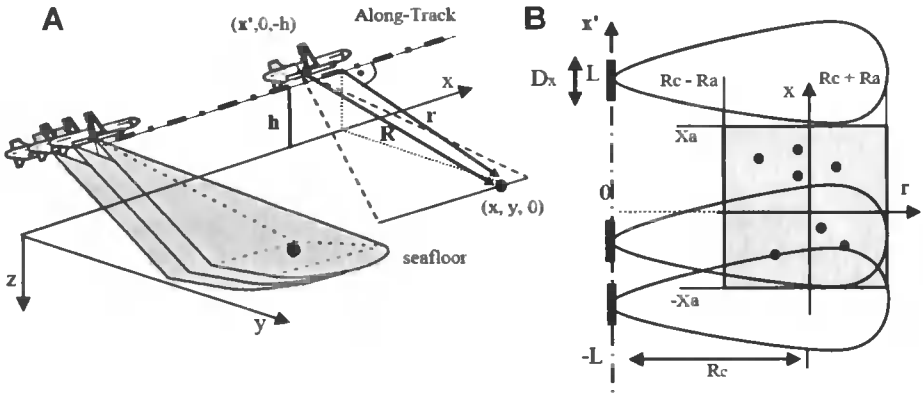


Fig. 1. Synthetic aperture imaging geometry: A) 3D; B) 2D

2. RANGE STACKING VS OMEGA-K

It is convenient to start with the mathematical model of the Omega-k algorithm and then go to the Range Stacking algorithm in order to show crucial differences. Taking advantage of the equation 3, we can write the SAS signal for the whole imaged area

$$e(\mathbf{x}', t) = \iint_{x r} \sigma(x, r) p \left(t - \frac{2\sqrt{(x - \mathbf{x}')^2 + r^2}}{c} \right) \exp \left[-i\omega_c \cdot \frac{2\sqrt{(x - \mathbf{x}')^2 + r^2}}{c} \right] dx dr \quad (4)$$

The aim of SAS processing is to determine the $\sigma(x, r)$ term which describes the desirable examined area reflectivity. Firstly, it's necessary to apply the Fourier transform on the raw SAS data. Using the simple rule $F_t[\delta(t - t_0)] = \exp(-i\omega \cdot t_0)$, where F_t is the forward Fourier transform with respect to time, we get SAS signal in the (\mathbf{x}', ω) domain

$$e(\mathbf{x}', \omega) = \iint_{x r} \sigma(x, r) \cdot P(\omega) \exp \left[-2i(\omega + \omega_c) \frac{\sqrt{r^2 + (x - \mathbf{x}')^2}}{c} \right] dx dr \quad (5)$$

$P(\omega)$ denotes the transformation of the transmitted sonar signal $p(t)$ defined in the equation (2). The next step is the transformation of this signal to the spatial frequency k_x domain by means of the Fourier transform with respect to the variable \mathbf{x}' in the form $F_{x'}[e(\mathbf{x}', \omega)]$. This problem can't be solved analytically. Fortunately, the above transform can be evaluated by means of the method of stationary phase in the following way

$$\begin{aligned}
 F_{x'} & \left[\exp \left(-2i(\omega + \omega_c) \frac{\sqrt{r^2 + (x - x')^2}}{c} \right) \right] \approx \\
 & \approx A \exp \left(-ir \sqrt{\left(\frac{2(\omega + \omega_c)}{c} \right)^2 - (k_{x'})^2} - ik_{x'} \cdot x \right)
 \end{aligned} \tag{6}$$

where A is a slowly-fluctuating scaling term and therefore, it can be ignored. The above equation leads us eventually to the following integral which is the two-dimensional Fourier transform of the received SAS data

$$e(k_{x'}, \omega) = \iint_{x r} \sigma(x, r) \cdot P(\omega) \exp[-ir \sqrt{\left(\frac{2(\omega + \omega_c)}{c} \right)^2 - (k_{x'})^2} - ik_{x'} \cdot x] dx dr \tag{7}$$

The Omega-k algorithm relies on the Stolt mapping defined below [1, 2]

$$k_r = \sqrt{\left(\frac{2(\omega + \omega_c)}{c} \right)^2 - (k_{x'})^2} \tag{8}$$

$$k_x = k_{x'} \tag{9}$$

After the mapping the expression (7) becomes

$$e(k_x, k_r) \iint_{x r} \sigma(x, r) \cdot P(\omega) \exp[-ik_r \cdot r - ik_x \cdot x] dx dr \tag{10}$$

Spatial frequencies k_x and k_r represent the wavenumber in the along-track direction and the range direction respectively. Therefore, Omega-k is often called wavenumber algorithm. In order to complete the discrete inverse Fourier transform (the next step of this algorithm) the data must be evenly spaced in k_x and k_r domain. The nonlinear nature of the equation (8) causes unevenly spaced data. Therefore, it is required an interpolation to make possible a further processing. To sum up: the consequence of the Stolt mapping is the necessity of an interpolation of the SAS data. A target function estimating desirable $\sigma(x, r)$ function (the approximation results from a limited band of the SAS signal) is obtained from the equation (10) in the following way

$$f_c(x, r) = \iint_{k_x k_r} e(k_x, k_r) \cdot P^*(\omega) \exp[ik_r \cdot R_c] \cdot \exp[ik_r \cdot r + ik_x \cdot x] dk_x dk_r \tag{11}$$

where $P^*(\omega)$ is the complex conjugate of $P(\omega)$. The additional term which has appeared in the above equations allows to bring this signal to the low pass, i.e. this operation lets us to center the resultant SAS image at the reference distance

R_c . According to Fig. 1B, R_c and X_c represent the center of the illuminated area in the range and along-track domains respectively. The described case is broad-side type, where $X_c=0$. If it is not, we should introduce the additional function in the form $\exp(ik_r X_c)$.

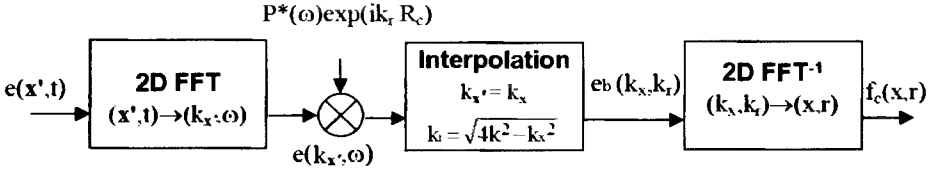


Fig. 2. Digital implementation of Omega-k algorithm

The Range Stacking algorithm allows to eliminate the Stolt mapping and thus an interpolation required in the Omega-k. The basic idea of this algorithm is the change of integral limits from (k_x, k_r) into $(k_{x'}, \omega)$ in the equation (11). It results in

$$\begin{aligned}
 f_c(x, r) = & \iint_{k_{x'} \omega} e(k_{x'}, \omega) P^*(\omega) \exp[i\sqrt{4k^2 - (k_{x'})^2} \cdot R_c] \cdot \\
 & \cdot \exp[i\sqrt{(4k^2 - (k_{x'})^2) \cdot r + ik_{x'} \cdot x}] \cdot J(k_{x'}, \omega) dk_{x'} d\omega, \quad (12) \\
 \text{where } J(k_{x'}, \omega) = & \frac{dk_r(\omega)}{d\omega} = \frac{4k}{c\sqrt{4k^2 - (k_{x'})^2}}
 \end{aligned}$$

is the slowly fluctuating Jacobian function which results from the applied transformation. It can be ignored because its contribution in the reconstruction is negligible. We may assume as well that this term and the previous amplitude function A are absorbed in the signal $e(k_{x'}, \omega)$.

Let's introduce the auxiliary function, being the received echo signal in $(k_{x'}, \omega)$ domain from an ideal point target located at the distance $R_c + r_k$ and situated on the r -axis (Fig. 1B)

$$e_{r_k}(k_{x'}, \omega) = P(\omega) \cdot \exp\left(-i(R_c + r_k)\sqrt{4k^2 - (k_{x'})^2}\right) \quad (13)$$

Then, the equation (12) can be rewritten as follows

$$\begin{aligned}
 f_c(x, r_k) &= \int_{k_{x'}} \left[\int_{\omega} e(k_{x'}, \omega) \cdot e^*_{r_k}(k_{x'}, \omega) d\omega \right] \cdot \exp(ik_{x'} \cdot x) dk_{x'} \\
 &= \int_{k_{x'}} \left[\int_{\omega} e(k_{x'}, \omega) \cdot P^*(\omega) \exp\left(i(R_c + r_k)\sqrt{4k^2 - (k_{x'})^2}\right) d\omega \right] \cdot \exp(ik_{x'} \cdot x) dk_{x'}
 \end{aligned} \tag{14}$$

In fact, the expression within square brackets is a matched filtering operation. The SAS signal is matched filtered with the reference function at the range r_k . Then, the outcome is integrated over the available fast-time frequencies ω to yield the marginal Fourier transform $F_c(k_{x'}, r_k)$. Applying the inverse Fourier transform with respect to $k_{x'}$ we get the target function $f_c(x, r_k)$ at the range r_k . The block diagram of the Range Stacking algorithm is depicted in Fig. 3. It is necessary to stress that shown steps have to be repeated for each range bin.

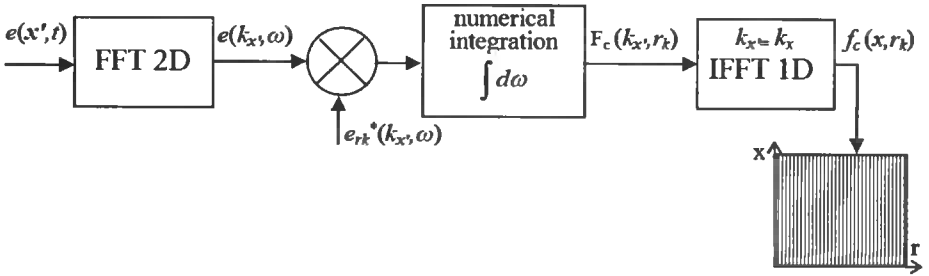


Fig. 3. Digital implementation of Range Stacking algorithm

3. COMPARISON CRITERIA

One possibility in order to specify a performance of a SAS system is to examine its impulse response. In such systems the impulse response can be obtained by measuring the system response to a single point target. As the result of the SAS reconstruction is two-dimensional image, quality parameters should be measured in two dimensions, azimuth and range. Because SAS impulse response is a sinc-like function, standard and well-known quantities such as **Impulse Response Width (IRW)**, **Peak SideLobe Ratio (PSLR)**, **Integrated SideLobe Ratio (ISLR)** were chosen as the quality parameters. The first one is the resolution measure and the others refer to contrast in a resultant image. In order to calculate the above parameters it is necessary to interpolate the SAS system impulse response firstly.

This is because a sinc-like function is represented by too few samples in a point target image (Fig. 4, the left image). The interpolation was carried out by centering the 32x32 window on the maximum of the main lobe and applying

zero padding in the frequency domain. The inverse Fourier transform IFFT with respect to the along-track and range directions gives the desirable image, appropriate to determine wanted parameters (Fig. 4, the right image). An additional comparison criterion was the difference graph of two normalized SAS images ($0 \leq \text{abs}[f_c(x,r)] \leq 1$) reconstructed by examined algorithms.

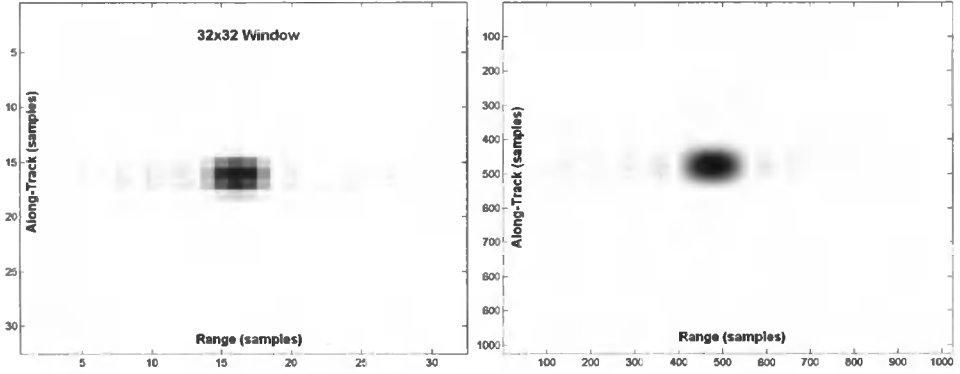


Fig. 4. SAS reconstruction of a point target: 32x32 window centered on the point target (left image); Interpolated point target (right image)

4. NUMERICAL SIMULATIONS

The assumed parameters of the stripmap SAS system are listed in Table 1. The raw SAS signals were generated for different point targets configurations in the imaged and simulated seafloor area. One of them is shown in Fig. 5A. The received SAS signals were next processed by the Omega-k and Range Stacking reconstruction algorithms to obtain high-resolution images of the illuminated area (Fig. 5B). Then, the 32x32 window was centered on each point target in the examined scene and parameters described in section 3 were calculated in order to compare the same point target processed by different reconstruction algorithms. Thanks to this it was possible to equate Omega-k to Range Stacking in following way

$$\delta = \frac{\text{Parameter_OmegaK} - \text{Parameter_RangeStacking}}{\text{Parameter_OmegaK}} * 100\% \quad (15)$$

Table 1. Assumed parameters of a stripmap SAS system

velocity of platform	0.5 [m/s]
c (sound speed in water)	1500 [m/s]
chirp bandwidth	5 [kHz]
chirp duration	5 [ms]
carrier frequency	100 [kHz]
PRF (Pulse Repetition Frequency)	15 [Hz]
D_x (sonar diameter in the along-track direction)	0.16 [m]
range resolution	0.0750 [m]
along-track resolution	0.0800 [m]
$2 * R_a$ (examined seafloor in the range direction)	20 [m]
$2 * X_a$ (examined seafloor in the azimuth direction)	10 [m]
R_c (distance to the center of the examined area)	30 [m]

The representative result of the comparison of two algorithms (for the SAS signal in figure 5A) is shown in Table 2. The main tool which allowed to emulate SAS system in the stripmap mode, to implement both algorithms, extract and prepare point target images, calculate suitable parameters and finally compare the obtained results was the Matlab environment.

Table 2. Relative differences δ (according to the equation 15) between parameters calculated for along-track and range profiles reconstructed by Omega-k and Range Stacking algorithms

Point Target	Along-Track Profile				Range Profile			
	PSLR	IRW 3 dB	IRW null-to-null	ISLR	PSLR	IRW 3 dB	IRW null-to-null	ISLR
1	-0.33	0	0	-0.24	0.27	0	0	0.15
2	0	0	0	0	0	0	0	0
3	0	0	0	0	0	0	0	0
4	0	0	0	0	0	0	0	0.02
5	0	0	0	0	0	0	0	0
6	0.03	0	0	0.04	-0.13	0	0	-0.38
7	0.39	0	0	0.33	0.18	0	0	-0.1
8	0.7	0	0	0.64	0.09	0	0	-0.05
9	0	0	0	0	0.04	0	0	0
10	0	0	0	0	0	0	0	0
11	0	0	0	0	0	0	0	0
12	0	0	0.66	-0.01	-0.04	0	0	0
13	-0.03	0	0	0	0	0	0	0
14	0	0	0	-0.03	0	0	0	0
15	0	0	0	-0.01	0	0	0	-0.03
16	0	0	0	0	0	0	0	0
17	0	0	0	0	0.04	0	0	0

Table 2 continued

18	0	0	0	0	0	0	0	0
19	0	0	0	0.01	0	0	0	0
20	-0.03	0	0	0.03	0	0	0	-0.03
21	0	0	0	0.01	0	0	0	0
22	0	0	0	0	0	0	0	0
23	0	0	0	0	0	0	0	0
24	-0.08	0	0	-0.06	0.04	0	0	0
25	0	0	0	0	0	0	0	0
26	0	0	0	-0.01	0	0	0	-0.03
27	0	0	0	0	0	0	0	-0.03
28	-0.03	0	0	-0.01	0	0	0	-0.03
29	0	0	0.65	-0.01	0	0	0	0.03
30	0	0	0	0.01	0	0	0	0
31	0	0	0	0	0	0	0	0
32	0	0	0	-0.03	0	0	0	0
33	0	0	0	0	0	0	0	0
34	0.03	0	0	0.03	0	0	0	-0.03
35	0	0	0	0.03	0	0	0	0
36	0	0	0	0	0	0	0	0
37	0.17	0	0.65	0.32	0.76	0	-1.14	0.73
38	-0.03	0	0	-0.01	0	0	0	0
39	0.39	0	-0.66	0.39	0.18	0	0	-0.1
40	0	0	0	0	0	0	0	0.03
41	0.03	0	0	0	-0.09	0	0	-0.23
42	0	0	0	0	0	0	0	0
43	-0.03	0	0	-0.08	-0.22	0	0	-0.33

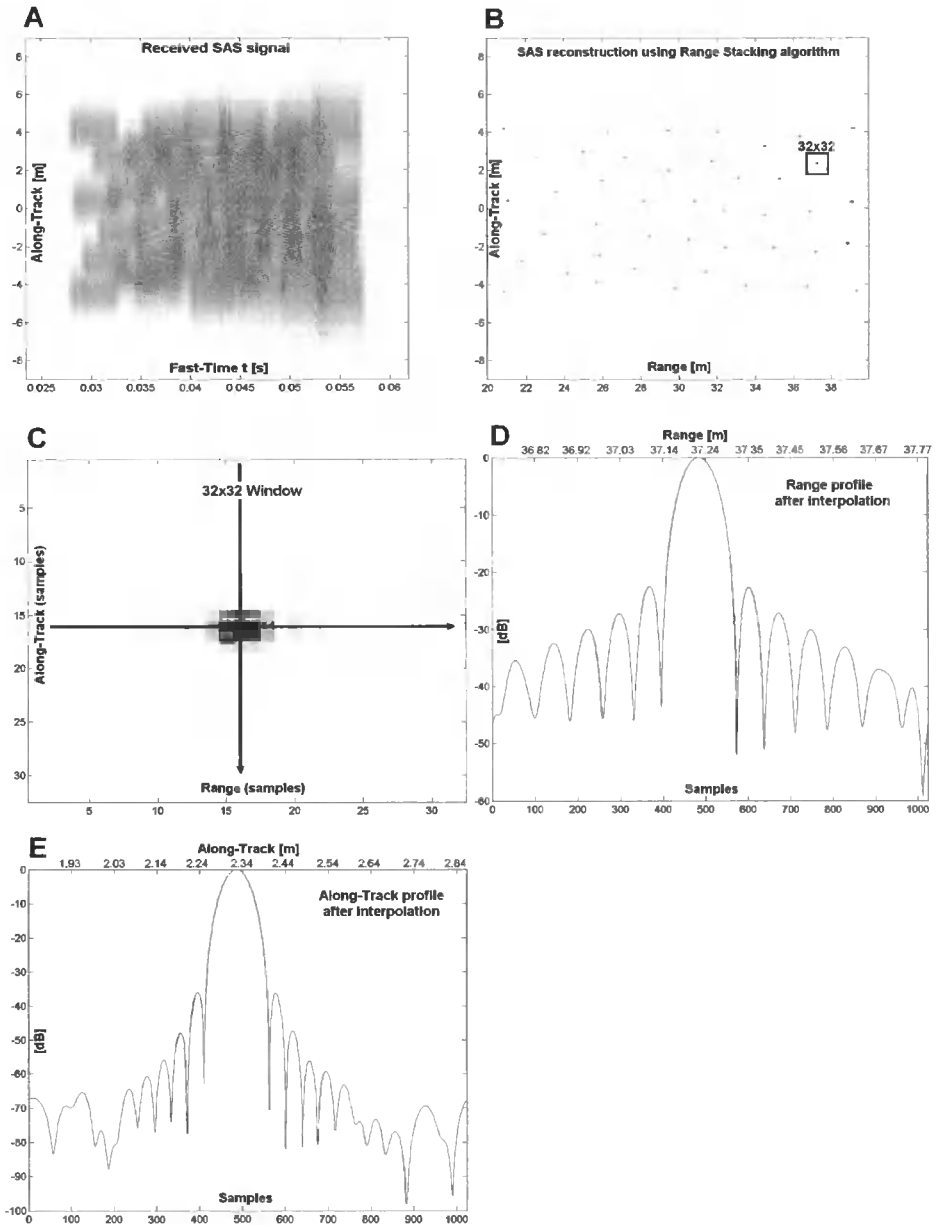


Fig. 5. Some results of the simulations: A) The Received raw SAS signal for 43 point targets; B) The resultant SAS image reconstructed by means of the Range Stacking algorithm; C) 32x32 window used to extract single point targets from the imaged scene; D, E) Range and along-track profiles retrieved by the Range Stacking processing and interpolated by zero padding in the frequency domain

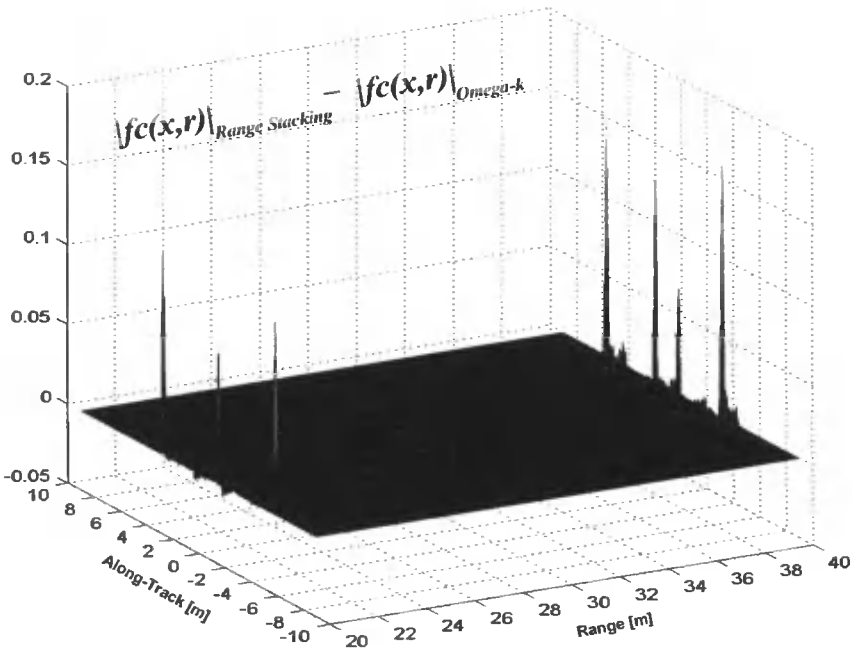


Fig. 6. Difference of two SAS images reconstructed by Range Stacking and Omega-k

5. SUMMARY AND CONCLUSIONS

More than a dozen SAS images containing point targets (randomly located in the illuminated scene) were examined. The square window was used to extract single point targets from reconstructed SAS images. The set of parameters (IRW, PSLR, ISLR) calculated on the basis of along-track and range profiles (Fig. 5D, 5E) of all point targets allowed to compare two different reconstruction algorithms, Range Stacking and Omega-k. The result of this comparison did not unambiguously indicate better algorithm. The examined relative differences δ were at very low level and did not exceed 2% (the maximum value for the SAS image in Figure 5A amounted to 1,13%). Despite occurring some differences, it seemed to be a little random because of appearing small positive and negative values in each column (e.g. Table 2) a comparable number of times. To recapitulate, it was difficult to note a clear trend here.

The opposite situation was with the interpretation of the difference graph of two normalized SAS images obtained by different reconstruction algorithms. As we can see in Figure 6, the biggest positive peaks (biggest differences) are at the edges of the graph. It means that these peaks in SAS images processed by Range Stacking algorithm have higher values what is undoubtedly its advantage. To be more precise, point targets on edges of the illuminated area are

better focused by the examined Range Stacking algorithm than Omega-k one. The graph in Figure 6 is a simple difference between two reconstructed SAS images $f_c(x,r)$ obtained by means of these two algorithms for exactly the same illuminated scene (point targets). This differential graph includes small negative peaks inside the area and bigger positive peaks at edges. Occurring small negative peaks are connected with the used normalization process ($0 \leq \text{abs}[f_c(x,r)] \leq 1$) of reconstructed SAS images (two different peaks were found as maximums and chosen for the normalization of two compared SAS images respectively). So, we can connect these low negative peaks with a "normalization constant" which is not particularly valuable for the comparison of these algorithms. However, higher positive peaks indicate clearly better focusing for point targets on edges when Range Stacking algorithm is applied (positive values here indicate this algorithm as a winner in focusing edge point targets because the Omega-k reconstructed image was subtracted from Range Stacking one).

Certainly, the drawback of the Range Stacking algorithm is its computational complexity. The processing of the SAS signal in Figure 5A by means of Matlab was almost 22 times longer than the Omega-k reconstruction. However, the unique feature of the Range Stacking algorithm allows to run the processing of each line $f(x,r_k)$ at the same time and thus significantly to accelerate the reconstruction step [2].

Applying a spatial filtering to the raw SAS signals with the use of Polar Format Processing did not have a significant influence on the comparison results. In this case, calculating some parameters was a little bit ambiguous because of appearing small distortions in a few point spread functions. However, almost identical distortions occurred in both Omega-k and Range Stacking reconstructed images. Therefore, it was not taken into account in the comparison process.

BIBLIOGRAPHY

- [1] Cumming I., Wong F., *Digital Processing of Synthetic Aperture Radar Data*, Artech House, Norwood 2005.
- [2] Soumekh M., *Synthetic Aperture Radar Signal Processing*, John Wiley & Sons, USA 1999.
- [3] Szczegieliński M., *Przetwarzanie Danych SAS Przy Pomocy Algorytmu Omega-K*, Proceedings of 52-th Open Seminar on Acoustics, pp. 111-114, Wągrowiec 2005.
- [4] Szczegieliński M., *Spatial SAS Signal Filtering by Means of Polar Format Processing*, Hydroacoustics, Vol. 9, pp. 191-198, 2005.

PORÓWNANIE ALGORYTMÓW OMEGA-K ORAZ RANGE STACKING W PRZETWARZANIU SAS

Streszczenie

Przetwarzanie SAS (Synthetic Aperture Sonar) jest wciąż rozwijane w kierunku lepszych, bardziej efektywnych oraz dokładnych algorytmów. Pożądane jest stosowanie algorytmów, które nie wprowadzają dodatkowych błędów z powodu aproksymacji fazy lub cyfrowej interpolacji danych. Jednym z takich algorytmów jest "Range Stacking". W artykule zaprezentowano jego krótką charakterystykę z wyróżnieniem jego wad i zalet w stosunku do innego, chętnie stosowanego algorytmu rekonstrukcji Omega-k. Wygenerowane sygnały SAS dla trybu "stripmap" zostały wykorzystane do praktycznego porównania obydwu algorytmów. Zbiór symulowanych obrazów SAS zawierał również sygnały przefiltrowane przestrzennie za pomocą algorytmu "Polar Format Processing". Wyniki numerycznych symulacji zostały zaprezentowane i przedyskutowane w artykule.

Słowa kluczowe: sonar z syntetyczną aperturą, range stacking, omega-k, porównanie

APPROACH TO QoS/QoE MONITORING AND PARAMETRIC MODEL FOR IPTV SERVICE

Łukasz Trzcianowski, Sławomir Kula

Institute of Telecommunications
Warsaw University of Technology
Nowowiejska 15/19, 00-655 Warsaw, Poland

Summary: The main purpose of this paper is to present approach to QoS/QoE monitoring and parametric model creation for IPTV service. Monitoring system was used to perform on-line monitoring both MPEG TS parameters and subjective assessments (MOS). The second part of this work present parametric model for IPTV service, which describes relationships between single network parameters such as: jitter, packet loss, packet corrupt and throughput and subjective/objective quality measures (MOS, MSE). Created model shows influence of modified network conditions on the perceived video quality for variety video sequences extracted from IPTV network stream. This work also presents methodology of tests and their results which can be used to estimate the perceived quality for changes associated with modification of single network parameters.

Keywords: IPTV, quality of service, quality of experience, optical network, parametric model, monitoring system

1. INTRODUCTION

Dynamic evolution of telecommunications services and multimedia oriented interactivity is the reason for creation of new applications. Their attractiveness from customer side is not only measured by the price but also by the quality. Service provider looks at the quality from the perspective of network parameters, whereas from user side much more important is his satisfaction with the service provided. For that purpose it is needed to create monitoring system that will allow users and operators to check the quality of service. In this paper authors present the quality monitoring methodology and preliminary results of its application in practice for IPTV service. To find out how network parameters affect quality measures it was needed to test dependencies between them. Mentioned relations are required to estimate end-to-end quality and user satisfaction. Created in this way "E-model" can be used not only for monitoring reasons but also as a reference in the network planning processes. At present, there are two parametric models standardized by ITU – T organization (ITU – T G.107 for telephony and ITU – T G.1070 for videoconference). None of them is related to

IPTV service, that is more complex because of integration with on demand services and ability to interact with users. In this paper authors present their "E-model" for IPTV service which was created based on test results which show relationships between modified single network parameters and quality measures which are associated with user satisfaction and signal degradation. Apart from that they also present approach to create model for all the parameters.

2. THE CONCEPT OF MONITORING THE QUALITY FOR IPTV SERVICE

In developing the monitoring the quality of IPTV service it is needed to consider both service provider and end-user needs. Designed based on that system should give the operator ability to find relationships between users' complaints and network events. For the provider more important are network and signal parameters and on the other hand client want to be satisfied from provided service. That is why monitoring has to include not only checking network parameters but also user satisfaction. For that reason monitoring device should be located on the user side. Monitoring system should be implemented as software solution in Set Top Box. This device in normal situation is needed to decode and display television programs. Authors found problems with access to STB system, so the implementation was done by using additional external devices and applications. Due to use of additional tools, implemented system cannot be applied universally as a commercial solution.

3. LABORATORY NETWORK (PON/FTTH)

In Institute of Telecommunications at Warsaw University of technology it is located the distribution-access part of FITL network over which operator Multimedia Polska S. A. provides triple play services such as: broadband Internet, VoIP and IPTV. All of them are transmitted in aggregated stream to OLT device (*FiberHome AN5116*) in which optical signal is divided into particular ONU devices (*FiberHome AN5116*). In these units signal is converted from optical form to electrical form and services are transitioned to appropriate ports on which services were configured. Television signal, associated with IPTV service is delivered to one of FE ports and later on this signal is decoded in Set-Top-Box device (*iCAN2810W*) and at the end it's displayed on the monitor. To receive television materials connection between monitor and STB was replaced by appropriate system (for monitoring reason) or computer with software which allows to receive and save IPTV content (for tests related to parametric model creation).

Laboratory network architecture is presented in the figure below (Fig. 1):

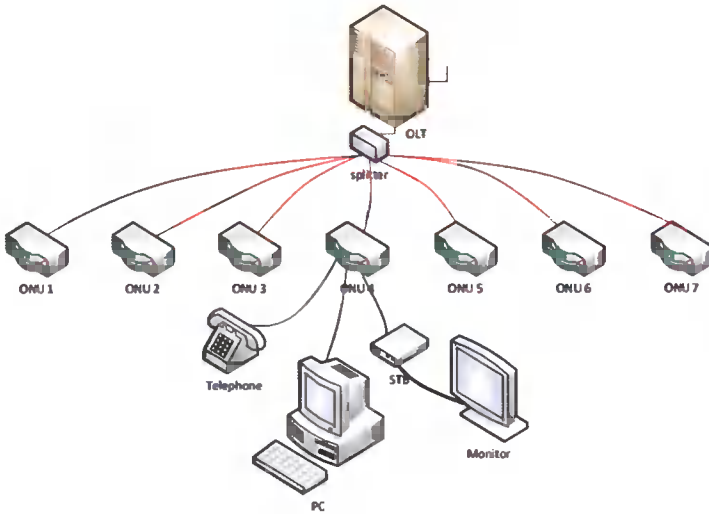


Fig. 1. Laboratory network scheme

4. MONITORING SYSTEM

Monitoring system was implemented at the end of laboratory network (Fig. 2). It connects PON/FTTH network and end-user devices.

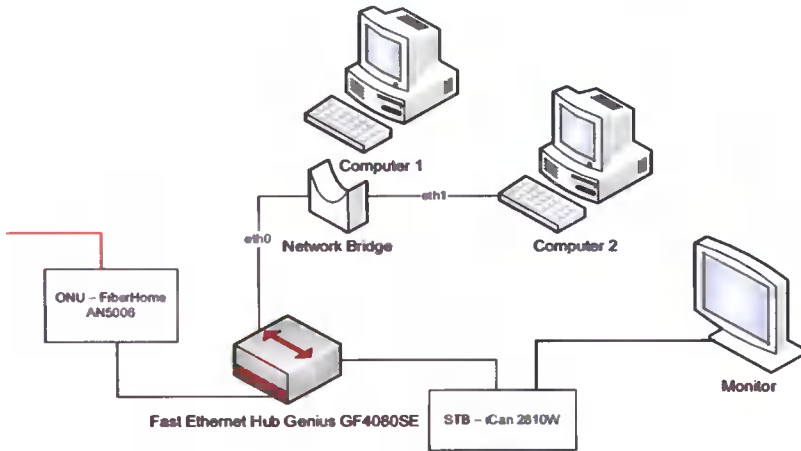


Fig. 2. Monitoring system scheme

Optical signal is transmitted over fibre to ONU device and then services are divided into particular Fast Ethernet ports. To monitor IPTV service authors

inserted Hub between ONU and Set Top Box. This device works at physical layer of the OSI model and it moves all network traffic from input port to output ports. One of Fast Ethernet ports was connected to STB, which by using HDMI connector provides video signal to monitor (*ASUS VH222D*) where it is displayed without any distortions. The same video signal from another Fast Ethernet port is transmitted to “Computer 1” that is responsible for changing network conditions according to settings. This device has two network interfaces: eth0 and eth1 connected by network bridge. Two ways of IPTV transmission allow to monitor distortions and degradations in real time. Created in this way monitoring system can be used not only to monitor parameters for received packets but also to check user satisfaction from provided service in various network states.

5. USED TOOLS – MONITORING TESTS

Agilent Triple Play Analyzer (ATPA)

This application is a software program allows to perform analysis and monitoring of the network traffic for Triple Play Services. In addition to the traffic statistics collection this tool can also determine and measure values typical for particular services. In case of IPTV service ATPA application can analyze parameters associated with MPEG TS and its components – PES (*Packetized Elementary Stream*).

MODTRAFNET

This custom-made application allows to automate the whole process associated with performing changes for particular network parameters. It is NETEM – based application with GUI interface. It supports the following network modifications:

- emulating delays determined by time value
- emulating jitter determined by average delay value and its variation
- emulating packet loss determined by percentage rate
- emulating packet reordering determined by delay value and by percentage values of changes.

VLC

VLC application is multimedia platform that allows to play audio and video files in various file formats such as: MPEG – 1, MPEG – 2, MPEG – 4, DivX, DVD, MP3, OGG. Application also supports streaming in both client and server role. It is also powerful server to stream live and on demand video in several formats/containers to Internet.

ANMS2000

ANMS2000 is dedicated management system for FiberHome devices. It can be used to manage AN5116-02 system including handling of equipment configuration, property, status, alarm and view. This tool was used to reduce the bandwidth for IPTV service in laboratory PON/FTTH network (please see 2).

6. MONITORING TESTS

This section describes monitoring tests and their results for given network conditions. The network changes were performed by setting appropriate values for the following parameters:

- packet loss
- packet corrupt
- bandwidth
- jitter

In case of MOS measures authors used commercial parametric model implemented in ATPA application.

Bandwidth

Bandwidth was modified by using ANMS2000 system which manages FTTH devices. This parameter was changed from 3 Mb/s to 10 Mb/s. Measurements were carried out using ATPA analyzer. Duration for signal sample was set on 10s and test duration was set on 100s. It allows to obtain appropriate accuracy without notable extension of testing time.

Reducing bandwidth parameter to 5 Mb/s doesn't cause any changes in the MPEG TS stream throughput. Fluctuations in the chart above (Fig. 3) are caused by various types of sequences transmitted in television (high motion, low motion sequences etc.). With the further gradual decreasing the bandwidth parameter the value of throughput for MPEG TS stream rapidly declined. For bandwidth parameter set on 4Mb/s users saw single distortions in received video and for bandwidth parameter set on 3 Mb/s service cannot be provided ("picture freezing effect"). Threshold for bandwidth limitations acceptance was defined as 4 Mb/s according to received MOS results.

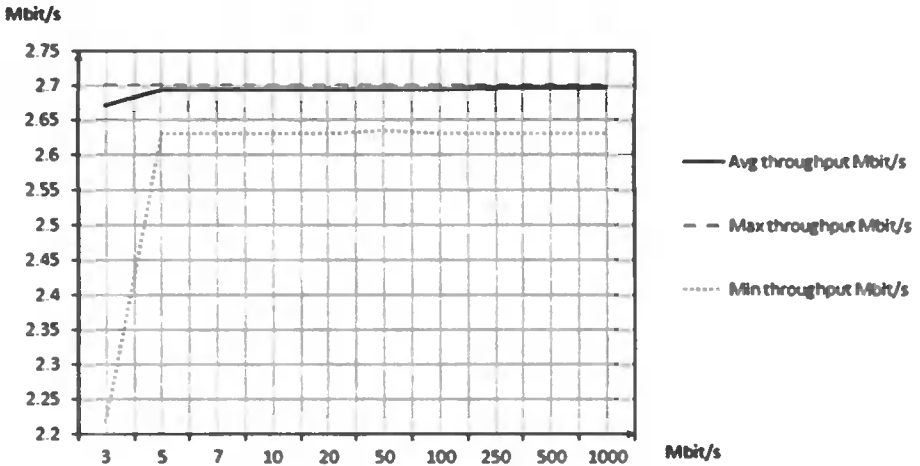


Fig. 3. MPEG TS stream – bandwidth modifications

Jitter (variability over time of the packet latency across a network)

Jitter parameter was modified by using MODTRAFNET application from 0 to 5 ms and average delay was set on 100 ms (Fig. 4). Measurements were carried out using ATPA analyzer. Tested measurements were: PCR jitter, MOS.

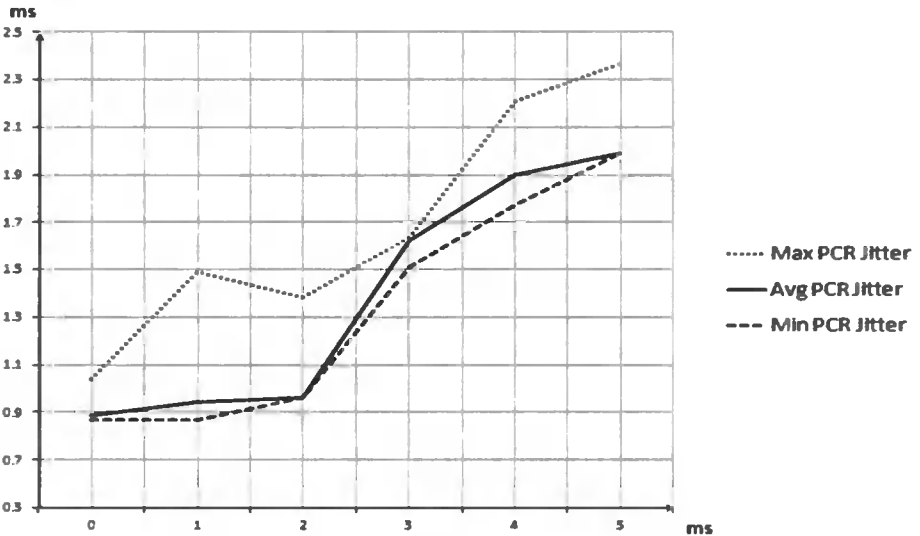


Fig. 4. PCR jitter – jitter modifications

Jitter has greater impact on the quality than the delay itself. Even a small values of this parameter can cause significant distortions at the video frame level what is related to problems with synchronization in the MPEG TS. The

big value of jitter cannot be compensated by buffers and it causes a lot of distortions in the video. Above chart shows that jitter is related to PCR parameter which is associated with synchronization between sound and video in MPEG TS. Indeed huge jitter has negative impact on this synchronization by causing errors which are very difficult to detection. Very good quality of video can be obtained till 3ms and limit of acceptability is 2 ms then MOS is greater or equal 4.

Packet loss

Packet loss parameter was modified by using MODTRAFNET application from 0 to 5% (Fig. 5). Packet were lost random (uniform distribution) without any correlation. Measured parameters were MOS and losses in MPEG TS stream.

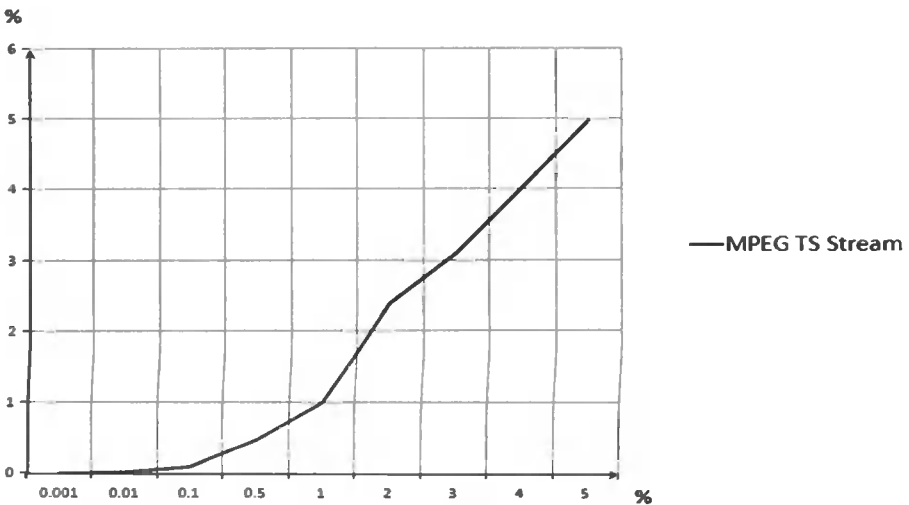


Fig. 5. MPEG TS packet loss – packet loss modifications

Packet loss in MPEG TS stream and general in the network traffic is comparable. Slight discrepancies are caused by additional packets f.e. related to network protocols SPT, IGMP etc. and also by various materials transmitted in the IPTV service (high and low motion sequences). Threshold of acceptability was defined as 0,1% of packet losses then MOS factor is still greater or equal 4.

Packet corrupt

Packet corrupt parameter was modified by using MODTRAFNET application from 0 to 5 %. Packet were corrupted random (uniform distribution) without any correlation same as in case of packet loss. Measured values were MOS and typical errors for MPEG TS such as: transport errors, sync byte errors, late PAT errors, PCR discontinuity errors.

Statistic of occurrence for these errors is presented in the chart below (Fig. 6):

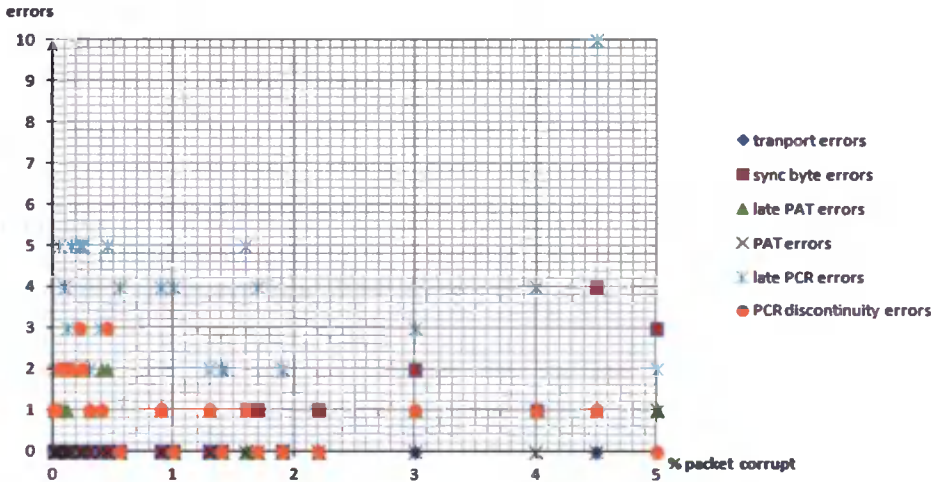


Fig. 6. MPEG TS packet corrupt – packet corrupt modifications

Errors are mainly random and the frequency of their occurrence depends on the length of the analyzed fields in MPEG TS stream (PES streams). For fields with larger length probability of damage is greater than for others f.e. “PCR” field is more frequently damaged than “Transport Error” field. The analysis of threshold acceptance for this parameter shows that 0,1% is acceptable value for packet corrupt, then MOS value is greater or equal 4.

7. PARAMETRIC MODEL – INTRODUCTION

In monitoring results presented in earlier sections the commercial parametric model implemented in TPA application was used. To verify if this model is correct for tested IPTV service authors created another model for standard quality measures: MOS, MSE. The main aim was to create parametric model for IPTV service which can show relationships between single network parameters and video signal quality.

8. TOOLS USED FOR PARAMETRIC MODEL CREATION

NETEM

NETEM is a network-simulator which provides Network Emulation functionality for testing protocols by emulating the properties of wide area network. Used version emulates the following changes:

- emulating delays determined by time value
- emulating jitter determined by average delay value and their variation
- emulating packet loss determined by percentage rate
- emulating packet reordering determined by delay value and by percentage values of changes.

In case of emulating modifications in network traffic it is possible to set percentage value of correlation, which determines relationships between the probability of occurrence particular modification in the next packet and current packet.

TBF linux application

TBF is a pure shaper and never schedules traffic. It is non-work-conserving and may throttle itself, although packets are available, to ensure that the configured rate is not exceeded. TBF can be described by the following parameters:

- limit (buffer),
- latency,
- MPU,
- burst,
- rate.

This tool is often used as bandwidth modifier for real-time applications.

MSU Video Quality Measurement Tool

Application MSU Video Quality Measurement Tool is a program for performing objective assessment. In set of available measures are : *MSE*, *PSNR*, *MSU* and *VQM*. Quality is determined by the comparison of input files, which can be in the following formats: *AVI*, *AVS*, *YUV* and *BMP*. MSU VQMT application has enhanced functionality such as: metric visualizations, saving particular frames from compared sequences etc. After finish of the process there is possible to determine the metric value by generating appropriate report in *.csv format.

MSU Perceptual Video Tool

MSU Perceptual Video is a tool for subjective video quality evaluation. With the use of this application it is possible to conduct subjective measurements with methods that are described in ITU – R BT.500 standard. Program can use 6 methods listed below:

- DSIS (*Double Stimulus Impairment Scale*),
- DSCQS (*Double Stimulus Continuous Quality Scale*) type 1 i 2,
- SCACJ (*Stimulus Comparison Adjectival Categorical Judgement*),
- EBU SAMVIQ (*Subjective Assessment Method for Video Quality evaluation*),
- MSUCQE (*MSU Continuous Quality Evaluation*).

Four of them are described in mentioned ITU recommendation. To perform tests it is necessary to create tasks (files with *.tsk extension). They consist of information about input files and comparison methods. After processing summary report can be generated (*.csv file).

VLC

(please refer to 4.)

9. TEST SYSTEM AND SAMPLES

Reference samples were extracted from IPTV television streams. Their duration was set on 10s. Samples were created to best present various content transmitted in video stream in IPTV service. They were extracted from the following SDTV channels: TVP1, TVP2, VoDInfo, am@zing. Limitation for the tests related to using only SDTV samples was caused by the fact that HDTV channels were encrypted by provider and it was not possible to decrypt them in VLC application.

Created reference samples with technical parameters are presented below (Fig. 7).

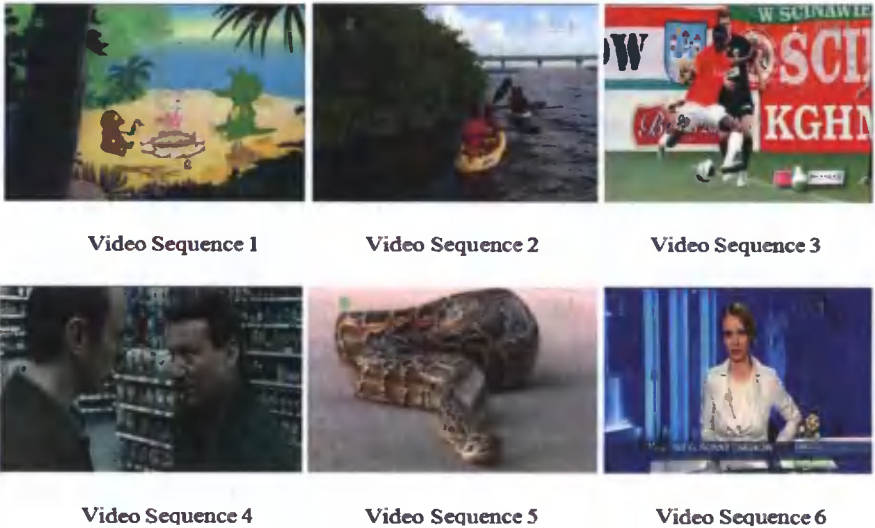


Fig. 7. Reference samples

Extracted from the stream reference probes (video signal fragments) had very good quality and subjective comparative tests with studio materials delivered by provider show that they are indistinguishable and that is why they could be used to generate test probes. For creating processed samples the following system was used (Fig. 8):

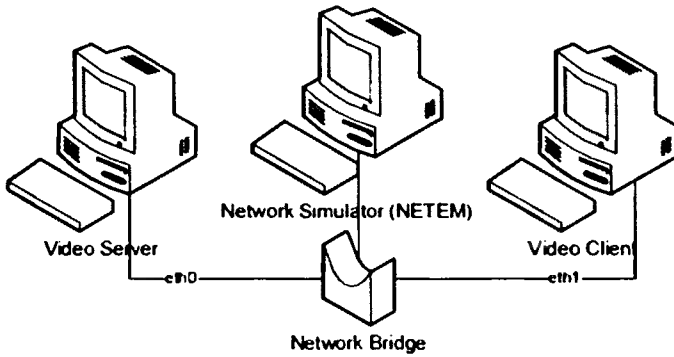


Fig. 8. Test system scheme

System consist of three computers. “Video Server” computer sent reference probes streamed in the network to “Video Client”. These probes in the next step were received and saved by “Video Client” creating new samples. Network traffic modification was performed by “Network Simulator” computer (it has two network interfaces which were connected by the network bridge). Modified parameters were: jitter, packet corrupt, packet loss and bandwidth. Generated from reference probes by appropriate modified network conditions probes were used as processed materials in subjective and objective quality tests.

10. TEST PROCEDURES

To determine parametric model for IPTV service using described in earlier sections reference and processed probes appropriate objective and subjective tests were performed. By analysis authors created dependencies which in the next step were used to create the model. In case of objective tests due to the nature of occurring changes it was chosen Mean Squared Error (MSE) and for subjective tests chosen metric was MOS in standard 5-stage scale. To measure these metrics authors used MSU Video Quality Measurement Tool and MSU Perceptual Video Tool for subjective tests (please refer to 7.). Subjective test were performed according to DSIS method. In the tests participated 20 people in different age groups (from 17 to 46). To increase the results reliability, they were trained about test procedures, used metrics, tools etc. In calculations of average value for MOS metric 95% was chosen. Received results and their analysis allow to determine dependencies between network parameters and chosen quality measures.

11. PARAMETRIC MODEL – JITTER

Jitter was modified by using NETEM tool. This parameter was changed from 0 to 5ms when average delay was set on 100 ms. Tested quality measures

were: MSE for objective tests and MOS for subjective tests (Figs. 9, 10). Tests show that jitter has a significant impact on the perceived quality especially when application buffer is set on small value. In objective tests degradation level most increased when jitter value was greater than 2 ms. The most rushing declines in subjective tests was observed in the range of values from 1 ms to 2 ms. First visible distortions were observed at the value of 1ms. It was also noted that negative changes in video caused by jitter modification has greater influence on high motion sequences.

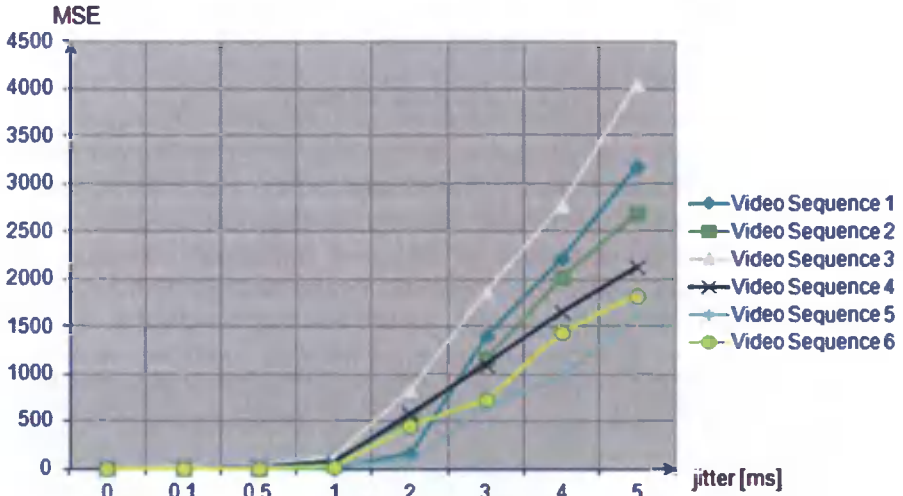


Fig. 9. Jitter – MSE

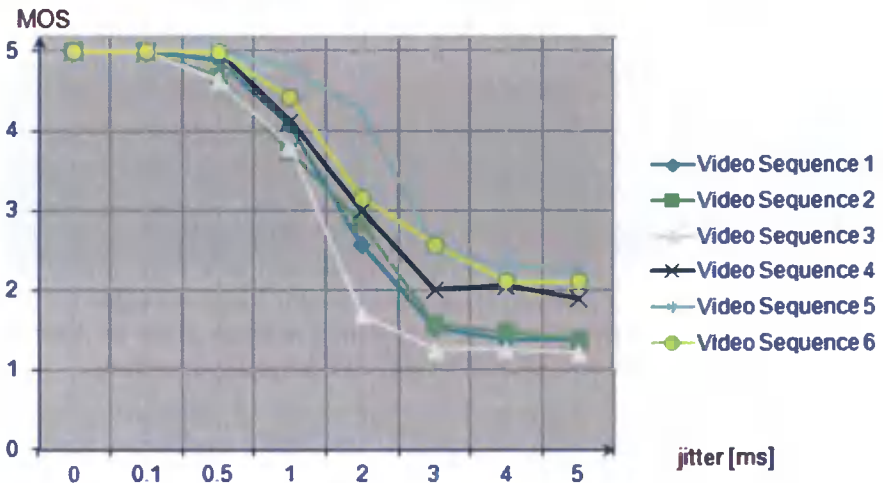


Fig. 10. Jitter – MOS

Dependencies for the worst case from presented in the charts above can be described by the following forms:

$$MSE = 119,08 \cdot (jtr[ms])^2 + 239,5 \cdot jtr[ms] - 70,652 \quad (1)$$

$$MOS = 0,0243 \cdot (jtr[ms])^5 - 0,3598 \cdot (jtr[ms])^4 + 1,8791 \cdot (jtr[ms])^3 - 3,778 \cdot (jtr[ms])^2 + 0,9175 \cdot jtr[ms] + 4,9668 \quad (2)$$

By analyzing the level of image degradation for delay variation it's possible to determine limiting value of this parameter above which degradations begin to have negative influence on the quality. For tested sequences the limit of acceptability for jitter is 1ms then MOS is greater or equal 4.

12. PARAMETRIC MODEL – PACKET LOSS

Percentage of packet loss was modified by using appropriate mechanisms of NETEM tool from 0% to 5%. Packets were lost random (uniform distribution) without correlation. The quality level was determined using Mean Squared Error metric for objective tests and MOS factor for subjective tests (Figs. 11, 12). Clearly more degraded were high motion sequences and less sensitive on changes in this parameter were slow motion sequences with small number of details. Additionally subjective tests showed that for the most sensitive sequence degradations are visible by users when level of packet loss is about 0,3%. The most common distortions are individual artifacts and blurring effects. For larger values of packet loss percentage it was possible to observe “freezing” effects in the playback picture. The negative effects intensified with the increase in the level of losses. Single, non-visible distortion, especially occurring in the background hasn't any negative impact on the subjective quality but long-lasting distortions cause customer irritation and in effect also low quality assessment.

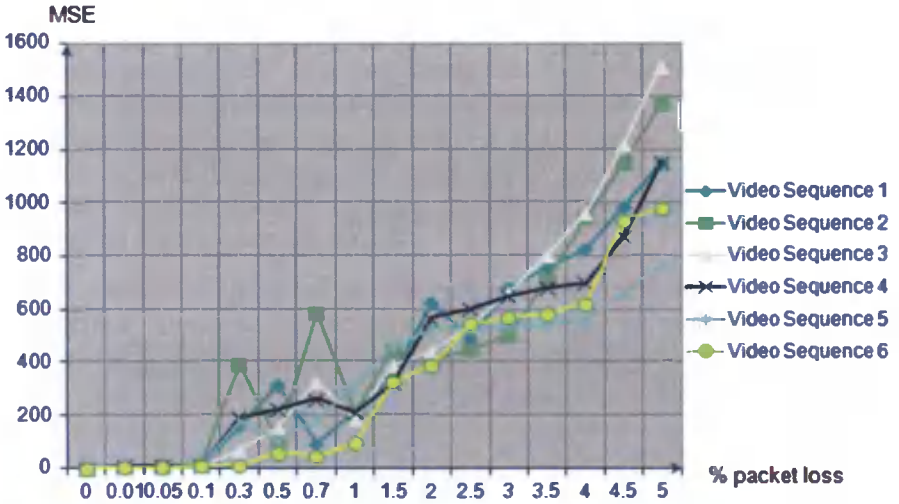


Fig. 11. Packet loss – MSE

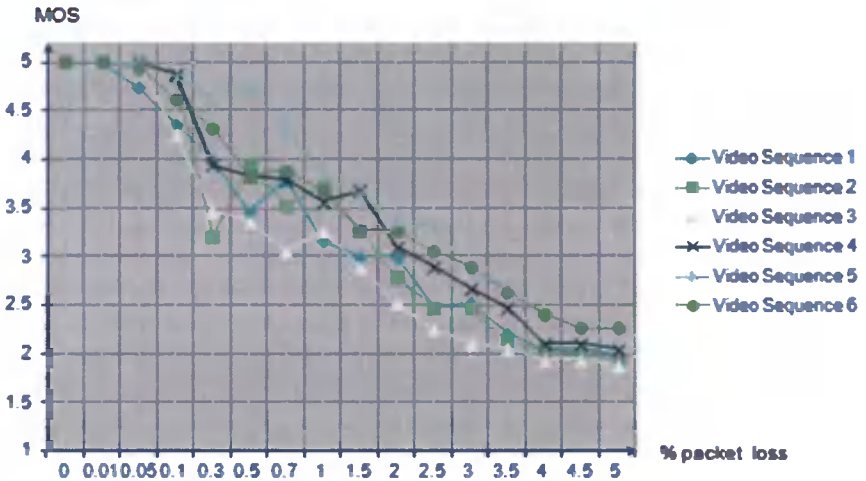


Fig. 12. Packet loss – MOS

Relationships for the worst case from tested can be described by the following forms:

$$MSE = 13,657 \cdot (p_loss[\%])^2 + 180,2 \cdot p_loss[\%] - 124,96 \quad (3)$$

$$MOS = 0,0132 \cdot (p_loss[\%])^2 - 0,4485 \cdot p_loss[\%] + 5,6634 \quad (4)$$

Analyzing received in objective and subjective tests values of quality measures and their dependencies allow to define acceptable level of packet loss. It was determined on the value of 1% packet loss.

13. PARAMETRIC MODEL – PACKET CORRUPT

Packet corrupt percentage value was modified from 0 to 5% (the same as in case of packet loss) by using appropriate mechanisms of NETEM application. Packet corrupt was performed by introducing bit distortion in the packet body. These distortions were creating random (uniform distribution) without any correlation. Measured metrics were: MSE for objective tests and MOS for subjective tests (Figs. 13, 14). The most detailed sequences were more sensitive to packet corrupt distortion than others. Less influenced in the tests were high motion sequences, however please note that these sequences were more degraded than low-motion probes. The nature of changes MSE for the next frames of particular sequence and its influence on the quality is similar to this received in packet loss tests. Here also level of degradation depends not only on amount of degraded data but also on their content. Errors in the “Intra” frames, even at lower amount of distortions may cause more degradations than for larger amount of destroyed data but when differential frames are damaged. It causes visible jumps of quality metric values in the charts. For the most sensitive sequences the first image distortions were visible for testers from 0.3% of distortions. Degradations, which mostly occurred are related to color bias, blurring and artifacts effect.

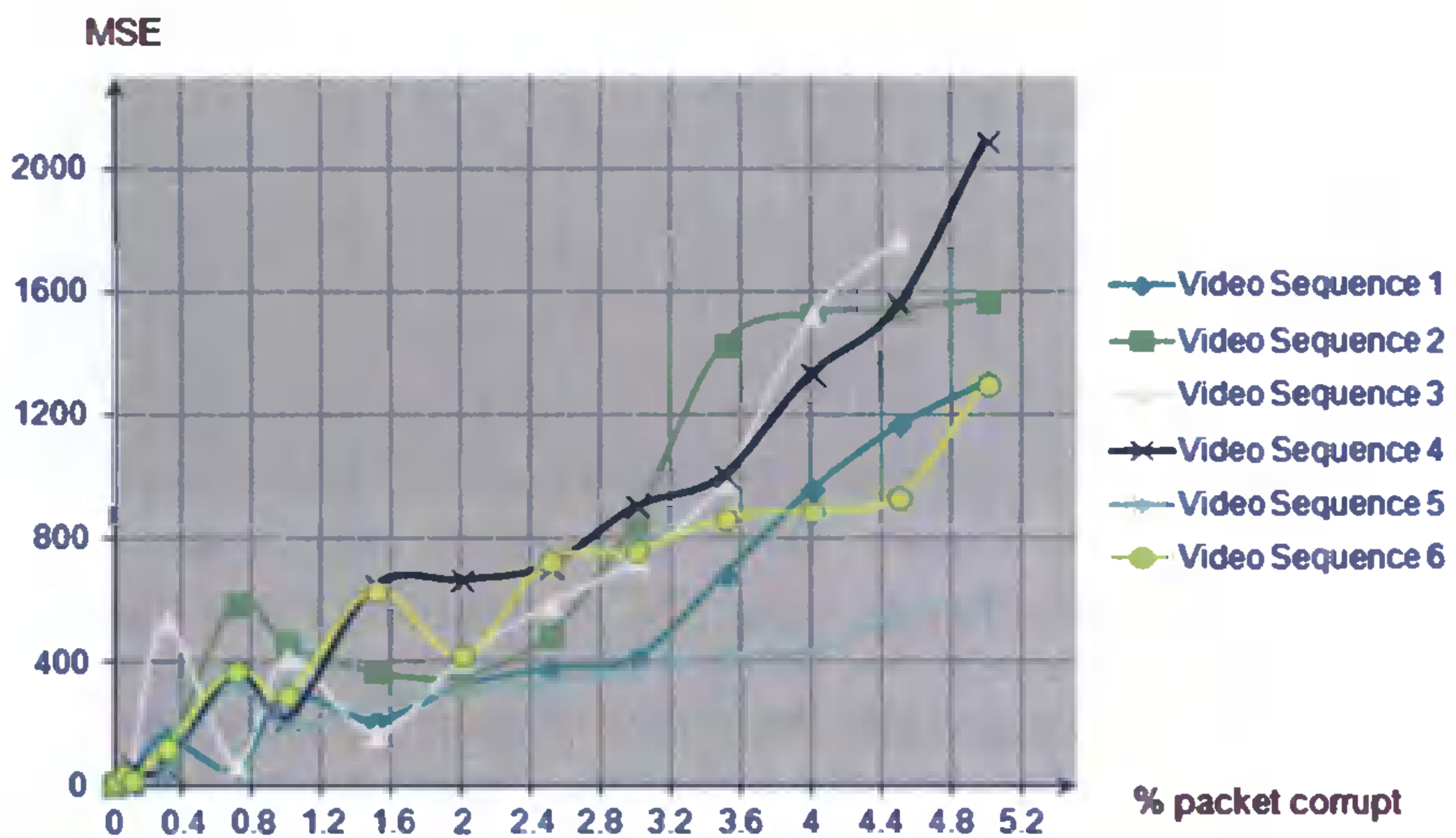


Fig. 13. Packet corrupt – MSE

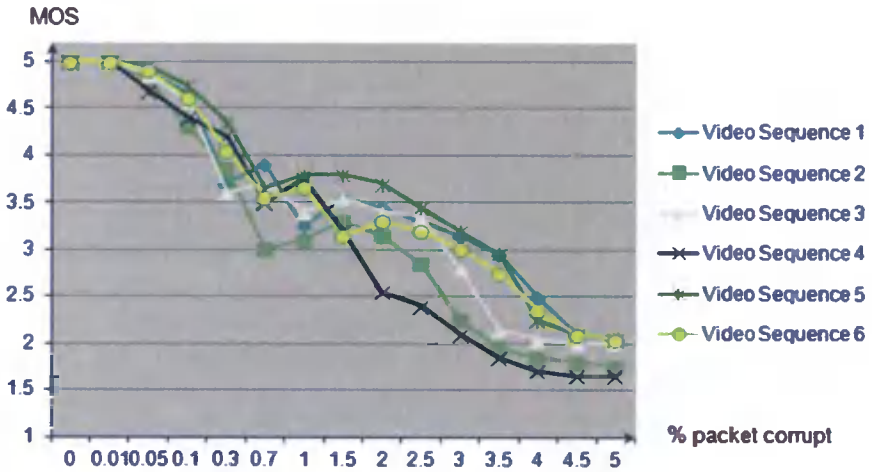


Fig. 14. Packet corrupt – MOS

Similar as in earlier examples received dependencies for all tested sequences were used to determine the worst case approximate functions, which can be described by using below forms:

$$MSE = 30,046 \cdot (p_corr[\%])^2 + 229,78 \cdot p_corr[\%] - 38,37 \quad (5)$$

$$MOS = -0,0001 \cdot (p_corr[\%])^4 + 0,0043 \cdot (p_corr[\%])^3 - 0,043 \cdot (p_corr[\%])^2 - 0,1959 \cdot p_corr[\%] + 5,3845 \quad (6)$$

Threshold for acceptance packet loss degradation was defined in test process as 0.1%.

14. PARAMETRIC MODEL – BANDWIDTH

Bandwidth was modified by using TBF mechanisms (Token Bucket Filter with shaper). This parameter was changed in depending on the sequence from value much more than maximum throughput of particular video sample to the value by which displaying cannot be performed. Chosen quality measures were: MSE for objective tests and MOS for subjective tests (Figs. 15, 16). Analysis shows that this parameter is critical for keeping quality on acceptable level. Limitations in value of this parameter have huge impact on quality degradation. Especially high-motion sequences are sensitive to negative effect caused by this parameter. Important was also maximum throughput. Distortions occurred due to TBF mechanisms were similar to those observed in large packet losing. Typical degradation when throughput value was insufficient for the service “picture freezing” occurred.

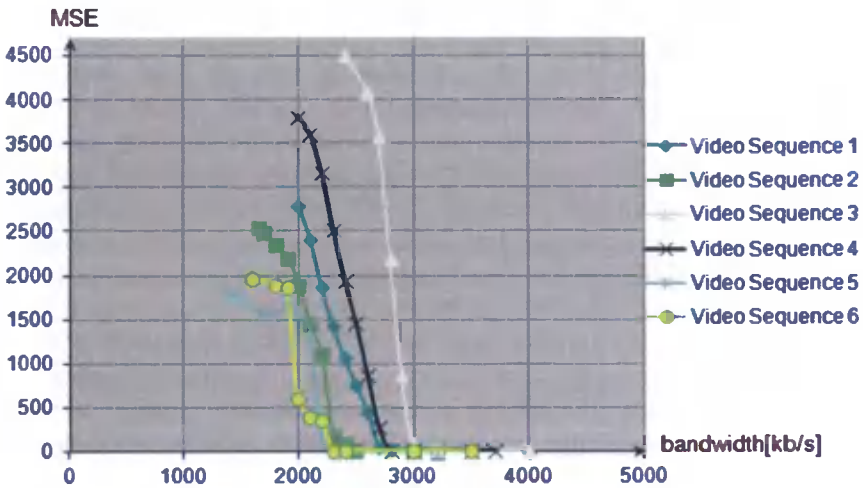


Fig. 15. Bandwidth – MSE

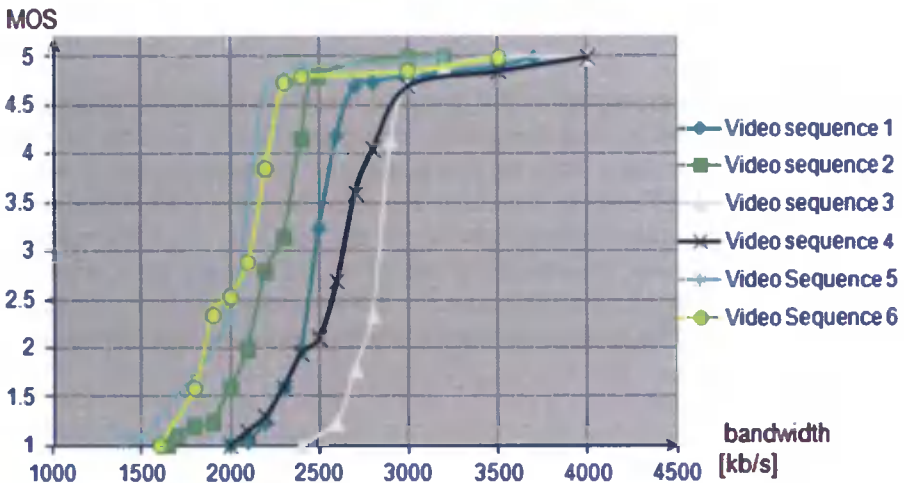


Fig. 16. Bandwidth – MOS

For all measured sequences the worst case can be described by the following forms:

$$MSE = 1,74 \cdot 10^{54} \cdot (thrp[kb/s])^{-14,87} \quad (7)$$

$$MOS = -3 \cdot 10^{-6} \cdot (thrp[kb/s])^2 + 0,0233 \cdot thrp[kb/s] - 37,171 \quad (8)$$

The analysis of the study threshold acceptance for this parameter shows that 3 Mb/s is acceptable bandwidth for IPTV service.

15. COMMON RELATIONSHIP – PROPOSED APPROACH

Presented test results show only dependencies between single network parameters such as: jitter, bandwidth, packet loss, packet corrupt and quality measures (MSE/MOS). To create common relationship between them it is needed to use statistics tools like analysis regression and correlation. Obviously it is necessary to have enough numbers of tests. After determining the correlation scatter plot between individual variables and quality measures it is needed to use correlation coefficient (chosen depending on data) to determine correlation. Then after finding relationships between variables it is needed to determine their nature. For this purpose it can be used graph of regression which is a statistical tool to determine the best-fit curve for set of points. This dependence should be determined for all combinations of network parameters and in effect it would be possible to define common relationship including dependencies between all network parameters and quality measures.

16. SUMMARY

Monitoring tests presented in this paper showed how network changes affect MPEG TS parameters and the quality - user satisfaction (MOS). Prepared parametric model is related only to single network parameters and it present dependencies between these parameters and quality measures for video signal in IPTV service. Additionally, authors introduced the concept of co-determination the impact of all network parameters to the service. The work associated with the development of the parametric model for IPTV service will be continued. In results this model can be used in network planning processes and also in monitoring quality systems.

BIBLIOGRAPHY

- [1] Hjelm J., 2008. Why IPTV? John Wiley & Sons.
- [2] Luther A.C., 1997. Principles of Digital Audio and Video, Artech House Norwood 05.
- [3] ITU – T E.800, Definitions of terms related to quality of service, 08/2008.
- [4] ITU – T G.107, The E-Model, a computational model for use in transmission planning, 05/2005.
- [5] ITU – T G.1070, Opinion Model For Video-telephony Applications, 11/2009.
- [6] ITU – R BT. 500 – 11, Methodology for the subjective assessment of the quality of television pictures, 06/2002.
- [7] ITU - T Y. 1540, Internet protocol data communication service - IP packet transfer and availability performance parameters, 12/2002.
- [8] ITU – T Y. 1541, Internet protocol data communication service – Quality of service and network performance objectives for IP-based services, 05/2002.

PODEJŚCIE DO USŁUGI MONITOROWANIA QoS/QoE I PARAMETRYCZNY MODEL DLA IPTV

Streszczenie

Głównym celem artykułu jest przedstawienie podejścia do monitorowania QoS/QoE i tworzenia modeli parametrycznych dla usługi IPTV. System monitorowania został użyty do monitorowania on-line parametrów (TS) MPEG i subiektywnej oceny (MOS). Druga część pracy prezentuje model parametryczny dla usług IPTV, który opisuje relacje między poszczególnymi parametrami sieciowymi, takimi jak: jitter, utrata pakietów, pakiety uszkodzone i przepustowość oraz subiektywnych/obiektywnych miar jakości (MOS, MSE). Stworzony model pokazuje wpływ zmiany warunków sieciowych na postrzeganą jakość wideo dla różnych sekwencji wideo pochodzących ze strumienia IPTV. Praca przedstawia również metodologię badań i wyniki, które można wykorzystać do oszacowania postrzeganej jakości zmian związanych z modyfikacją poszczególnych parametrów sieciowych.

Słowa kluczowe: IPTV, jakość usług, jakość doświadczeń, sieci optyczne, model parametryczny, system monitoringu

OBJECTS RECOGNITION SYSTEM WITH NEURAL NETWORK

Marcin Szczegielniak, Damian Szczegielniak


University of Technology and Life Sciences,
Kaliskiego 7, Bydgoszcz 85-796 Poland
szczegielniakm@wp.pl, dszczeg@utp.edu.pl

Summary: The system to recognize objects was designed and tested in the specialized application created and implemented by authors for neural networks and image processing simultaneously. This paper covers mathematical foundations of applied images standardization to achieve versatile and the invariant system to objects transformations (translation, scaling, rotation) in input images. Experiments with photos of objects were carried out and results were presented and discussed below.

Keywords: object recognition, image processing, neural network

1. INTRODUCTION

Artificial neural networks are used in many aspects or stages of the objects recognition. They can be applied not only as a classifier but for initial processing, segmentation or extracting objects features [7, 8]. There are many different types of artificial neural networks from classical structures to the newest ones which are still being developed [1, 6, 7]. However, this paper focuses on the versatile and popular multilayer feedforward perceptron as the features extractor and classifier simultaneously.










Network		
	Design Network	Window for designing the structure of the neural network.
	Define Image Processing	Windows for designing an image processing.
	Training Set	Window which allows to define a training set.
	Training Set Average Error	Graph of the mean square error for the training set.
	Test Trained Network	Window to test trained and ready networks.
Utility		
	Source Code Generator	It generates the Java code for a trained network (including designed image processing). This code can be used in any another Java application.
	Image Processing Toolbox	It opens the window of the image processing toolbox.

Fig. 1. Some functions available in the created application

The created specialized application allows for a robust and effective training of the network as well as to define a necessary initial images processing for the object recognition system. Although the aim of this paper is not to describe authors' application, Figures 1 and 2 may give only an idea how the environment of carried out experiments looks like. Further information is presented in next sections.

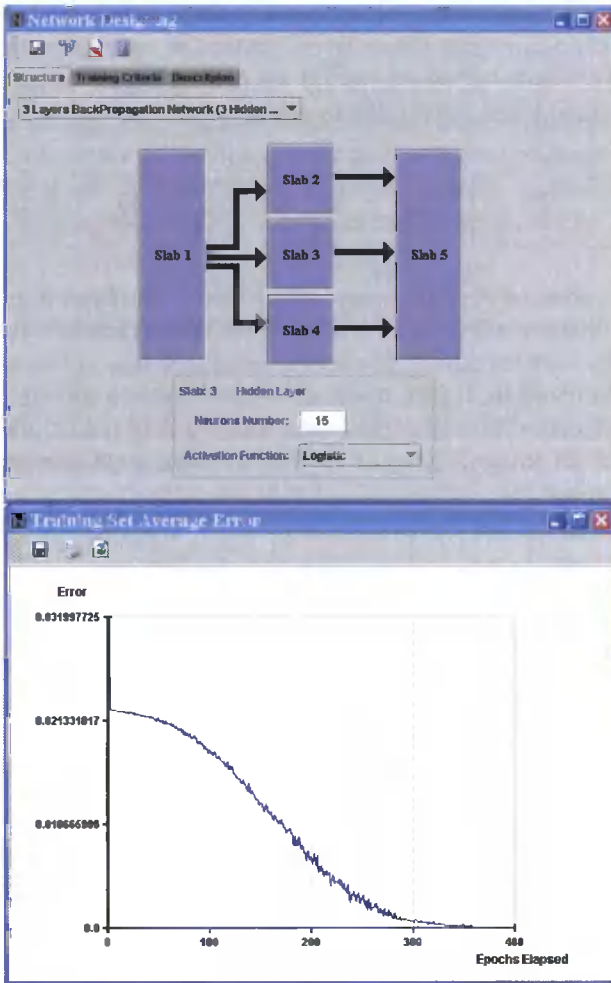


Fig. 2. Network designing and error preview during a training process

2. STANDARDIZATION OF INPUT IMAGES

It was assumed that a neural network was to extract some features of recognized input images on its own. Therefore, it is necessary to apply a proper initial processing which would allow a neural network to learn and work efficiently. It seems to be obvious that all possible variations of an object to recognize (with different sizes, rotations and positions in the input image) are too big set and should be reduced in a way before passing this image to the neural network. Therefore, a standardization of input images which makes an object independent of its translation (in X and Y directions), rotation and scale in the input image scene is executed first.

One of possible solutions [6] relies on cascade processing depicted in Figure 3. It is worth noting that the order of particular operations described below is important. This order allows to avoid exceeding bigger objects in the image beyond image boundaries during the rotation.



Fig. 3. Standardization of the input image which makes an object in processed images invariant to the translation (T block), scaling (S block) and rotation (R block)

The standardization T (the translation block) relies on finding a center of gravity of an object in the image and then moving it to the origin (assumed as a central point of an image). Thanks to this we can make the processed image translation-invariant [3].

We can calculate the center of gravity of a binary image in the following way

$$x_m = \frac{1}{P} \sum_{i=1}^N \sum_{j=1}^N x_i \cdot f(x_i, y_j) \quad (1)$$

$$y_m = \frac{1}{P} \sum_{i=1}^N \sum_{j=1}^N y_j \cdot f(x_i, y_j) \quad (2)$$

where

$$P = \sum_{i=1}^N \sum_{j=1}^N f(x_i, y_j) \quad (3)$$

is the number of pixels with the value 1. The function $f(x_i, y_j)$ is the binary image with values 0 for the background and 1 for the object. We can describe this operation as

$$f_T(x_i, y_j) = f_T(x_i + x_m, y_j + y_m) \quad (4)$$

The aim of the scaling (S) block is to make the input image scale-invariant, a recognized object should be always the same size after this processing. It changes the size of an object in order to make the average distance between the origin and 1-valued pixels equal of a fraction of an average size of the image frame. The average distance can be described by

$$r_m = \frac{1}{\sum_{i=1}^N \sum_{j=1}^N f_T(x_i, y_j)} \sum_{i=1}^N \sum_{j=1}^N f_T(x_i, y_j) \sqrt{x_i^2 + y_j^2} \quad (5)$$

A scale factor is specified by following equation

$$S = \frac{r_m}{R} \quad (6)$$

where R is an assumed fraction of the size of the image frame. This factor has to be chosen in order to avoid exceeding objects in the image beyond image boundaries (taking into account the next step - rotation as well). We assumed the value $\frac{1}{4}$ of this parameter. This operation can be described as

$$f_{IS}(x_i, y_j) = f_I(S \cdot x_i, S \cdot y_j) \quad (7)$$

The aim of the last rotation (R) block is to rotate an object to a standard/canonical position and make the processed image rotation-invariant simultaneously. To be more precise, this processing rotates an object in order to cover the direction of the maximum covariance with x-axis. For the two-dimensional image the covariance matrix is

$$C = \left(\frac{1}{P} \sum_{i=1}^N \sum_{j=1}^N f_{IS}(x_i, y_j) \begin{bmatrix} x_i \\ y_j \end{bmatrix} \begin{bmatrix} x_i \\ y_j \end{bmatrix}^T \right) - \begin{bmatrix} m_x \\ m_y \end{bmatrix} \begin{bmatrix} m_x \\ m_y \end{bmatrix}^T \quad (8)$$

where

$$P = \sum_{i=1}^N \sum_{j=1}^N f_{IS}(x_i, y_j) \quad (9)$$

and

$$\begin{bmatrix} m_x \\ m_y \end{bmatrix} = \frac{1}{P} \sum_{i=1}^N \sum_{j=1}^N f_{IS}(x_i, y_j) \begin{bmatrix} x_i \\ y_j \end{bmatrix} \quad (10)$$

Because m_x and m_y are equal zero (thanks to T block, the result of moving the center of gravity to the origin), the covariance matrix after neglecting the factor P is

$$C = \begin{bmatrix} T_{xx} & T_{xy} \\ T_{xy} & T_{yy} \end{bmatrix} \quad (11)$$

where

$$T_{xx} = \sum_{i=1}^N \sum_{j=1}^N x_i^2 \cdot f_{IS}(x_i, y_j) \quad (12)$$

$$T_{yy} = \sum_{i=1}^N \sum_{j=1}^N y_j^2 \cdot f_{IS}(x_i, y_j) \quad (13)$$

$$T_{xy} = \sum_{i=1}^N \sum_{j=1}^N x_i \cdot y_j \cdot f_{IS}(x_i, y_j) \quad (14)$$

The matrix eigenvalues C can be described by

$$\lambda_{1/2} = \frac{1}{2} \left[T_{yy} + T_{xx} \pm \sqrt{(T_{yy} + T_{xx})^2 - 4(T_{yy} \cdot T_{xx} + T_{xy}^2)} \right] \quad (15)$$

The eigenvector connected with the matrix eigenvalue is

$$C \begin{bmatrix} v_1 \\ v_2 \end{bmatrix} = \lambda \begin{bmatrix} v_1 \\ v_2 \end{bmatrix} \quad (16)$$

On the basis of the equation 15 we get the gradient of the eigenvector

$$\frac{v_1}{v_2} = \frac{\lambda - T_{xx}}{T_{xy}} \quad (17)$$

Taking into account equations 15 and 17 we have then

$$\frac{v_1}{v_2} = \frac{T_{yy} - T_{xx} + \sqrt{(T_{yy} - T_{xx})^2 - 4T_{xy}^2}}{2T_{xy}} \quad (18)$$

Functions $\sin(\Theta)$ and $\cos(\Theta)$, corresponding this gradient, are respectively

$$\sin(\Theta) = \frac{v_2}{\sqrt{v_1^2 + v_2^2}} = \frac{T_{yy} - T_{xx} + \sqrt{(T_{yy} - T_{xx})^2 - 4T_{xy}^2}}{M} \quad (19)$$

$$\cos(\Theta) = \frac{v_1}{\sqrt{v_1^2 + v_2^2}} = \frac{2T_{xy}}{M} \quad (20)$$

where

$$M = \sqrt{8T_{xy}^2 + 2(T_{yy} - T_{xx})^2 + 2(T_{yy} - T_{xx})\sqrt{(T_{yy} - T_{xx})^2 - 4T_{xy}^2}} \quad (21)$$

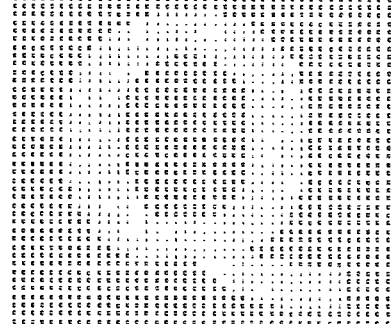
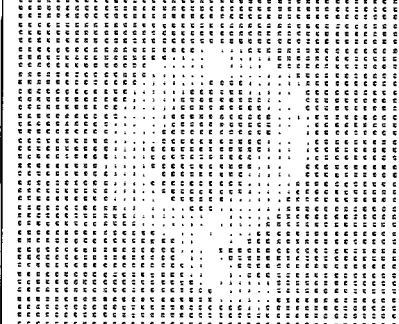
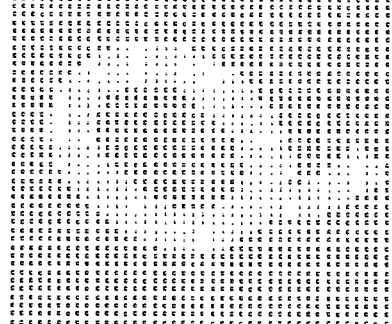
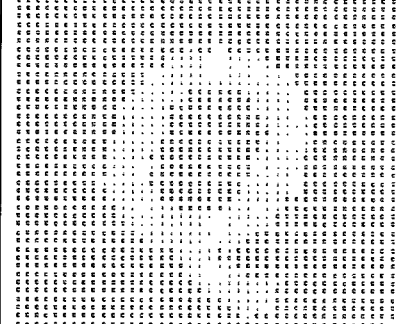
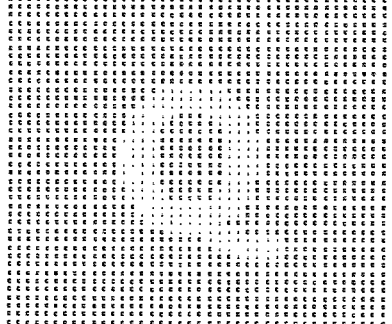
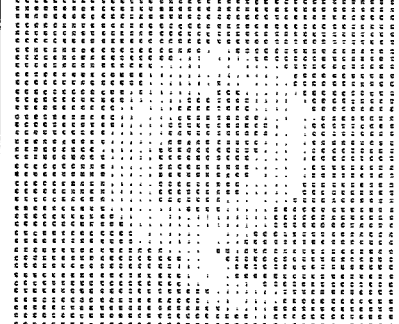
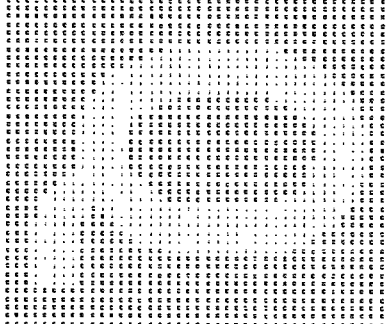
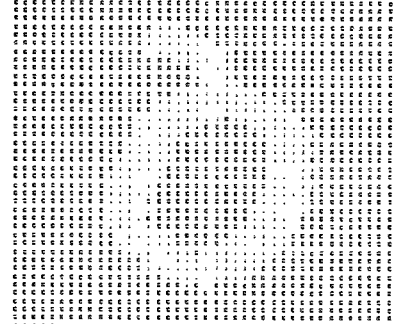
To sum up, the function projecting the image f_{TS} into f_{TSR} becomes

$$f_{TSR}(x_i, y_j) = f_{TS}(\cos(\Theta) \cdot x_i - \sin(\Theta) \cdot y_j, \sin(\Theta) \cdot x_i - \cos(\Theta) \cdot y_j) \quad (22)$$

It is worth mentioning that this projection doesn't recognize the direction and therefore, depending on the original object position in the image, the processed image f_{TSR} can take one of two possible canonical positions, representing the same object. It has to be taken into account during the preparation of training patterns for the neural network.

In the table 1 there were a few examples of the standardization of an image described above. The standardization in the last case $Q+90^\circ.jpg$ resulted in the second possible canonical object position.

Table 1. Examples of the image standardization (input images in the left column and resultant standardized images in the right one)

<p>Q.jpg</p>		
<p>Q-45 °.jpg</p>		
<p>Qsmall.jpg</p>		
<p>Q+90 °.jpg</p>		

3. RECOGNITION SYSTEM WITH NEURAL NETWORK

The proposed recognition system with the neural network was depicted in Fig. 4. A binary input image is standardized according to the processing described in section 3. Thanks to this an object in the standardized image can only be in one of two possible canonical positions which are invariant to the translation, scale and rotation of an object in the input image. Then the standardized image with the size $M \times M$ is reduced to $N \times N$ matrix, where $N < M$. The aim of scaling down the image is to reduce the structure of the neural network and further computational complexity. The input signal of the neural network is created by passing the input $N \times N$ matrix in the proper way (Fig. 4). It yields the input vector with N^2 elements.

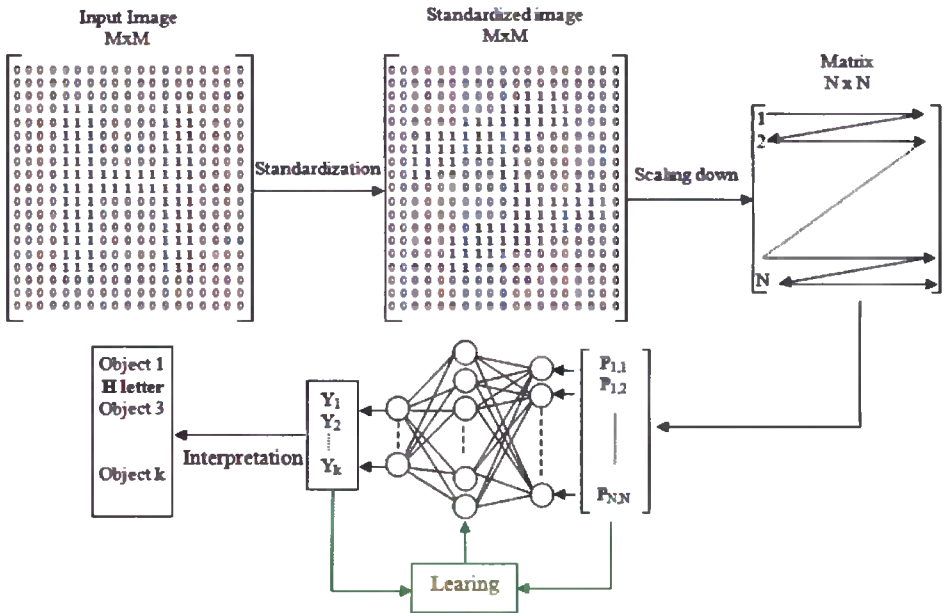


Fig. 4. Recognition system scheme

The number of neural network outputs was constant and depends on the number of recognized classes. The number of hidden neurons was only chosen during the training process (in order to ensure an ability to generalize but to avoid an excessive specialization in irrelevant details in the input image) [2]. The neural network with one hidden layer was trained on the basis of training set with the use of the backpropagation method. After the completed training process the neural network was ready to start working in the final recognition mode. In this mode every standardized input image processed by the neural network stimulated its output neuron, corresponding to the recognized class. The response of the neural network was interpreted and a decision about assigning the object into a recognized category/class (or about a lack of the recognition) was made.

4. INITIAL IMAGE PROCESSING AND RESULTS OF EXPERIMENTS

The described solution with the standardization of input images and the artificial neural network (the multilayer perceptron) as the features extractor and classifier simultaneously was applied in the carried out experiments. The aim was the recognition of objects from photos (showed below) which were divided into the training set (used only during training the neural network) and the test set (used to evaluate an effectiveness of this system). The test set includes photos of the same objects but these photos were taken from a little bit different perspective and with a different lighting. Both sets were increased by their modified versions, including objects scaled down (30% and 60% for the training set and 45% and 75% for the test set) and rotated (72° , 144° , 216° , 288° for the training set and 108° and 252° for the test set).



Fig. 5. Base images of the training set

Because the standardization of input images works properly only for binary images it is necessary to apply an initial processing of prepared photos sets. One of possible solutions of the initial images processing which allowed to achieve good results during carried out experiments is depicted in Figure 6. Following stages of the initial processing were applied before the standardization block.

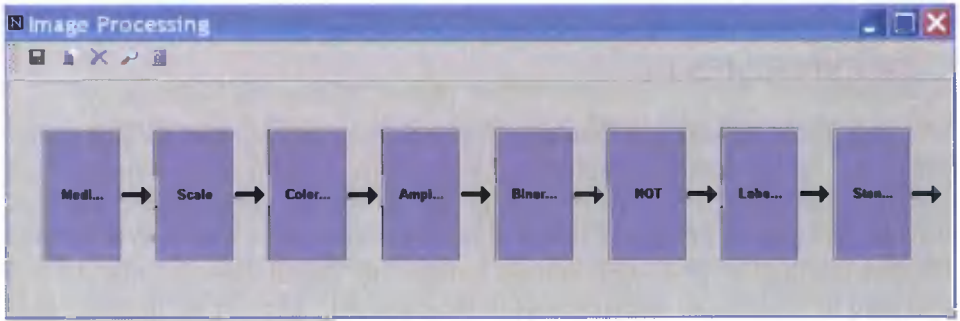


Fig. 6. Initial processing

First of all, an input image is passed by the median filter in order to remove the unfavorable noise (at a minimal change of the right image content which is an advantage of this filter). Next, the image is scaled down to the resolution 150x150 in order to reduce the computational complexity of further processing. Then the processed color image is changed into gray one and its contrast is enhanced (Color to Gray and Amplitude Rescaling blocks). The next step is the binarization (Binarize block). The NOT block ensures the proper representation of object pixels (value 1 for recognized objects, 0 for the background).

Finally, the image is labeled in order to distinguish and choose a correct object to recognize from other artifacts (Labeling block). Images processed this way are standardized (Standardization block) and passed to the neural network. An example of this processing, step by step, is depicted in Fig. 7.








The neural network with one hidden layer, containing neurons with logic activation functions, was trained on the basis of the training set and then the effectiveness of this trained network was checked with the use of the test set. During this process the number of hidden neurons was specified. It turned out that only 3 hidden neurons allowed the trained neural network to work properly.

Assuming that a signal of the output neuron, indicating the valid and reliable recognition of an object, should exceed signals on other outputs minimum 0.45 (a two-level interpretation) the effectiveness of the classification on the test set (which wasn't used in the training process) achieved 100%. Some results for particular input images were presented in the table 2. This recognition system worked very well even with very small objects with different locations or with objects which are not used in the training process or test set at all but belonged to one of recognized classes (for example, different screwdrivers marked in the table 2 with green descriptions).



Fig. 7. An example of the initial image processing

Table 2. Responses of the trained neural network for the test set

Image	Winner	Neural network output value	Distance to maximum level of other outputs
	Big screwdriver	"screw driver"	0.9413
	Socket wrench rotated and scaled down 75%	"socket wrench"	0.9790
	Pliers rotated and scaled down 75%	"pliers"	0.9903
	Small screwdriver	"screw driver"	0.9614
	Socket wrench rotated and scaled down 45%	"socket wrench"	0.8868
	Pliers rotated and scaled down 45%	"pliers"	0.9780
	Another type of screwdriver	"screw driver"	1.0

5. REMARKS AND CONCLUSIONS

The examined system with the initial image processing is the solution where the neural network works as the features extractor and classifier simultaneously. No additional algorithm for an extraction of objects features was needed. On the basis of carried out experiments it can be concluded that the applied neural network completed these tasks very well.

The system was insensitive to objects translation, scale and rotation in the input image (recognitions were correct thanks to applying the standardization of input images describe in this paper) and dealt with even with very small objects (scaled down 75%) in input images or with photos of objects taken at different lighting conditions and from a little bit different perspective. The system also recognized objects which belonged to one of the recognized classes but were not used in the training/test sets (marked with green in the table 2) which can confirm that the neural network was designed and trained properly because it had a generalization ability.

It seems to be obvious that this recognition system works well for a higher frequency noise or distortions. The input image is scaled to the matrix 15x15 before passing to the neural network. This scaling process reduces some details of the recognized objects (for example, as in Figure 7). It may be regarded as its advantage because of a distortions resistance. On the other hand, it may cause problems with a recognition of very similar objects but belonging to different classes. It is kind of trade off. However, it is always possible to increase the input matrix to allow the neural network to extract subtler features of objects at the expense of a higher computational complexity.

Generally, it is worth noting that the recognition of prepared test images (which were not used in the training process) worked perfectly in the designed system and it could perhaps prove correct in some real applications (for example, in a production process to recognize some parts automatically).

Certainly, it would be interesting to examine an influence of different kind of image distortions on the recognition process, especially that the neural network extracts features on its own. Authors are going to do this in future experiments.

BIBLIOGRAPHY

- [1] Jeatrakul P., Wong K.W., 2009. Comparing the Performance of Different Neural Networks for Binary Classification Problems. Eighth International Symposium on Natural Language Processing, pp. 111-115.
- [2] Kotsiantis S.B., Zaharakis I.D., Pintelas P.E., 2007. Supervised Machine Learning: A Review of Classification Techniques. Informatica, vol. 31, pp. 159-190.
- [3] Manjunath T.C., 2010. Detection of Shapes of Objects Using Sophisticated Image Processing Techniques. International Journal of Computer Science & Emerging Technologies, Volume 1, Issue 4, pp. 32-37.
- [4] Masters T., 1996. Sieci neuronowe w praktyce. Programowanie w języku C++. Wydawnictwa Naukowo-Techniczne.
- [5] Osowski S., 1996. Sieci neuronowe. Oficyna Wydawnicza Politechniki Warszawskiej.

- [6] Osowski S., 1997. Sieci neuronowe w ujęciu algorytmicznym. Wydawnictwa Naukowo-Techniczne.
- [7] Osowski S., 2006. Sieci neuronowe do przetwarzania informacji. Oficyna Wydawnicza Politechniki Warszawskiej.
- [8] Zhang G.P., 2000. Neural Networks for Classification: A Survey. IEEE Transactions On Systems, Man, And Cybernetics - Part C: Applications And Reviews, vol. 30, No. 4, pp. 451-462.

SYSTEM ROZPOZNAWANIA OBIEKTÓW Z WYKORZYSTANIEM SIECI NEURONOWYCH

Streszczenie

W pracy zaprojektowano i przetestowano, w zaimplementowanej przez autorów specjalistycznej aplikacji, system do rozpoznawania obiektów oparty na technice sieci neuronowych i zaawansowanym wstępnym przetwarzaniu obrazów. Praca obejmuje matematyczne podstawy standaryzacji przetwarzanych obrazów wejściowych, zastosowanej do osiągnięcia uniwersalnego i inwariantnego systemu, niezależnego od transformacji obiektów (przesunięcia, skalowania, rotacji). W pracy przedstawiono i omówiono wyniki przeprowadzonych eksperymentów z wykorzystaniem zdjęć zawierających testowe obiekty.

Słowa kluczowe: rozpoznawanie obiektów, przetwarzanie obrazów, sieci neuronowe

ISSN 1899-0088